

HDL-TR-1811

13

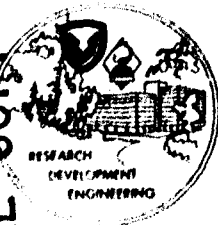
AD A043192

Simulation of Sequential Setback and Aerodynamic Drag of Ordnance Projectiles

JUNE 1977

HDL TR 1811 - Simulation of Sequential Setback and Aerodynamic Drag of Ordnance Projectiles, by Irvin Pollin

**U.S. Army Materiel Development
and Readiness Command
HARRY DIAMOND LABORATORIES
Adelphi, Maryland 20783**



DC FILE COPY

NO. 1

The findings in this report are not to be construed as an official Department of the Army position unless so designated by other authorized documents.

Citation of manufacturers' or trade names does not constitute an official indorsement or approval of the use thereof.

Destroy this report when it is no longer needed. Do not return it to the originator.

UNCLASSIFIED

SECURITY CLASSIFICATION OF THIS PAGE (When Data Entered)

REPORT DOCUMENTATION PAGE		READ INSTRUCTIONS BEFORE COMPLETING FORM
1. REPORT NUMBER 14 HDL-TR-1811	2. GOVT ACCESSION NO.	3. RECIPIENT'S CATALOG NUMBER 9
4. TITLE (and Subtitle) Simulation of Sequential Setback and Aerodynamic Drag of Ordnance Projectiles.	5. TYPE OF REPORT & PERIOD COVERED Technical Report.	
7. AUTHOR(s) 10 Irvin/Pollin	8. CONTRACT OR GRANT NUMBER(s)	
9. PERFORMING ORGANIZATION NAME AND ADDRESS Harry Diamond Laboratories 2800 Powder Mill Road Adelphi, MD 20783	10. PROGRAM ELEMENT, PROJECT, TASK AREA & WORK UNIT NUMBERS	
11. CONTROLLING OFFICE NAME AND ADDRESS US Army Materiel Development & Readiness Command Alexandria, VA 22333	12. REPORT DATE 11 June 1977	13. NUMBER OF PAGES 43
14. MONITORING AGENCY NAME & ADDRESS (if different from Controlling Office) 12 37p. 11	15. SECURITY CLASS. (of this report) UNCLASSIFIED	
16. DISTRIBUTION STATEMENT (of this Report) Approved for public release; distribution unlimited.		
17. DISTRIBUTION STATEMENT (of the abstract entered in Block 20, if different from Report)		
18. SUPPLEMENTARY NOTES HDL Project: 800685 DRCMS Code: 5391.OH.192400		
19. KEY WORDS (Continue on reverse side if necessary and identify by block number) Interior ballistics Safety and arming Setback Fuzing Aerodynamic drag Impact pulse shapes Artillery simulation Ordnance projectiles		
20. ABSTRACT (Continue on reverse side if necessary and identify by block number) Various testers are used at the Harry Diamond Laboratories to provide simulation of artillery interior ballistic environments (setback, angular acceleration) and exterior ballistic environments (spin, aerodynamic drag). This paper describes the work performed to combine setback and drag into a single laboratory tester to simulate these environments sequentially, as they would occur in real launch.		

REC'D
AUG 22 1977
MILITARY

DD FORM 1 JAN 73 1473

EDITION OF 1 NOV 65 IS OBSOLETE

UNCLASSIFIED

1 SECURITY CLASSIFICATION OF THIS PAGE (When Data Entered)

163 050

13

UNCLASSIFIED

SECURITY CLASSIFICATION OF THIS PAGE (When Data Entered)

A variety of pulse shapes has been obtained (in this simulator and in other simulators used for setback only) with peak accelerations of 300 to 100,000 g (acceleration of gravity) at impact speeds up to 1500 ft/s (460 m/s) and energies up to 55,000 ft-lb (7600 m-kg). The present tests attained maximum setbacks of 5000 g with a pulse duration of 1.5 ms. A steady-state drag commenced within 4 ms of the completion of setback, and aerodynamic drag up to 30 g was simulated for periods up to 20 ms. Good agreement between test and predicted data was found for both setback and drag. Independent of setback, the simulation of aerodynamic drag can readily be extended to larger drags, longer time periods, or specific drag-time profiles. Data are presented on simulator tests of an Army fuze mechanism which requires both setback and drag to arm.

UNCLASSIFIED

2 SECURITY CLASSIFICATION OF THIS PAGE (When Data Entered)

CONTENTS

	<u>Page</u>
1. INTRODUCTION	5
2. SIMULATOR DESIGN	6
3. COMPUTER PROGRAMS	10
3.1 Setback for Aluminum Mitigators	14
3.2 Drag	15
4. THEORETICAL AND EXPERIMENTAL RESULTS	16
4.1 Setback	16
4.2 Drag	17
4.3 Safety and Arming Device Tests	30
5. SUMMARY AND CONCLUSIONS	32
SYMBOLS	33
APPENDIX A.--CODES	35
DISTRIBUTION	37

ACCESSION for

NTIS

DDC

White Section

Buff Section

ANNOUNCED

CLASSIFICATION

BY

DISTRIBUTION/AVAILABILITY CODES

of SPECIAL

A		
---	--	--

FIGURES

1	Setback drag simulator	6
2	Setback drag simulator (schematic)	6
3	Projectile ("bird") and safety and arming device	8
4	Aluminum honeycomb and wood mitigators	9
5	Momentum exchange masses and washers	10
6	Calculated and experimental setback data for aluminum honeycomb mitigators (shots 113 and 118 to 120)	12
7	Experimental setback data for wood mitigators (shots 108 and 110 to 112)	13
8	Precision of drag measurements	19
9	Calculated and experimental drag data for aluminum honeycomb mitigator ($A_7 = 0.432 \text{ in.}^2$; shots 116 to 118)	23
10	Calculated and experimental drag data for aluminum honeycomb mitigator ($A_7 = 0.241 \text{ in.}^2$; shots 119 and 120)	24

FIGURES (Cont'd)

	<u>Page</u>
11 Calculated and experimental drag data for aluminum honey-comb mitigator ($A_7 = 0.117 \text{ in.}^2$; shots 113 and 114) . . .	25
12 Calculated and experimental drag data for wood mitigator ($A_7 = 1.443 \text{ in.}^2$; shots 111, 112, 121, and 122)	26
13 Calculated and experimental drag data for wood mitigator ($A_7 = 0.622 \text{ in.}^2$; shots 109, 110, 123, and 124)	27
14 Calculated and experimental drag data for wood mitigator ($A_7 = 0.432 \text{ in.}^2$; shots 107, 108, 125, and 126)	28
15 Calculated and experimental drag data for wood mitigator ($A_7 = 0.241 \text{ in.}^2$; shots 101, 102, 104, and 105)	29
16 Calculated and experimental drag data for wood mitigator ($A_7 = 0.117 \text{ in.}^2$; shots 99 and 100)	30

TABLES

I Test Values Used in Simulation of Drag and Setback . . .	7
II Effects of Initial Cavity Pressure and Volume on Aerodynamic Drag	20
III Test Record of Performance of Fuze Safety and Arming Device	32

1. INTRODUCTION

In the simulation of the sequential setback and aerodynamic drag, the projectile (called a bird), having equipment on board to be test evaluated, emerges from a launcher (typically a gas gun) and impacts an aluminum honeycomb or wood mitigator located between the bird and a momentum exchange mass (MEM). The equipment in the bird is mounted so that the impact simulates the setback pulse (acceleration-time trajectory) that occurs in the weapon launcher. The drag signature is simulated thereafter. Test data of the bird displacement as a function of time are obtained by a streak photograph, from which the setback and drag are determined by double differentiation. The conservation equations of mass, momentum, and energy are solved exactly to obtain the forces acting on and the motions of the bird, mitigator, and MEM as functions of time.

The setback comprises essentially three parts: rise, steady, and fall. The rise and steady parts occur during the crushing of the mitigator, and their characteristic features are determined primarily by the bird mass and by the shape, dynamic crush strength, and mass density of the mitigator. The fall is controlled primarily by the elasticity of the components at maximum mitigator crush; this may include the elasticity intentionally introduced into the system, by incorporating springs into the MEM. By this means, parabolic, trapezoidal, and other pulse shapes have been obtained.

The drag simulation is obtained as follows: The bird emerges from the gas gun, and impact occurs within an open-ended catch tube of circular cross section (fig. 1, 2). (The bird and MEM are circular cylinders.) The bird forms a close fit with the inner wall of the catch tube. However, the diameter of the MEM is selected to obtain a desired air leakage into the cavity formed by the bird, tube, and MEM. (The mitigator diameter is small enough not to obstruct air flow between the bird and the MEM.) The setback pulse is designed so that the bird velocity at the completion of setback is approximately zero, and the bird momentum is transferred to the MEM. The MEM motion increases the length of the cavity, causing the cavity pressure to drop, and gives rise to a pressure differential across the bird. The bird acceleration, or drag simulation, is therefore determined primarily by the relative motion between the bird and the MEM, the cavity volume, the air leakage into the cavity, and the bird mass. The MEM mass is much larger than the bird mass so that little change in the MEM speed occurs during drag simulation. Pressure buildup in the cavity during a setback is minimized by the longitudinal slotted opening to the atmosphere in the catch tube that extends from the point where the bird enters the tube to a position near where the bird impacts the mitigator. The drag profile is not significantly changed by moderate variations of the initial cavity volume and pressure.

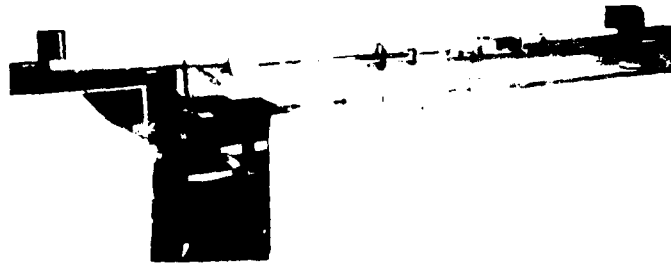


Figure 1. Setback drag simulator. 552-76

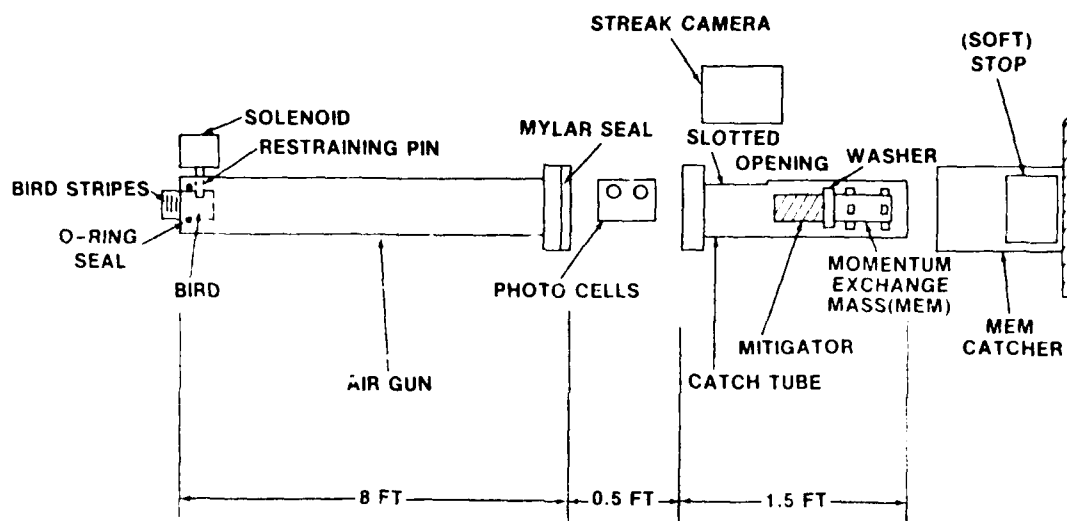


Figure 2. Setback drag simulator (schematic).

2. SIMULATOR DESIGN

In the present tests,* a Harry Diamond Laboratories (HDL) gas gun 2.5 in. (6.4 cm) in diameter and 8 ft (2.4 m) long was used in combination with a catch tube 2.5 in. (6.4 cm) in diameter and 1.5 ft (0.46 m) long to provide the sequential simulation of the setback and drag environments (fig. 1, 2). The gas gun is sealed at one end by the bird and by a 0.002-in (0.005-cm) Mylar diaphragm at the other end. A

*The concept of the simulator and much of its design are the work of Herbert Curchack. Arthur Ball and Robert Kayser built the device. Robert Kayser, Forrest Nelson, and Don Mary operated the simulator and obtained test data. Herbert Curchack and Don Mary reduced the streak photograph data. Kathy Mott prepared this typescript.

vacuum of about 1 Torr (100 Pa) is drawn in the space between the seals; and, upon release of a restraining pin, the bird is driven the length of the gun and into the catch tube by atmospheric air. In each of 30 tests, the 0.53-kg bird emerged from the gun at a speed of 155 ± 5 ft/s (47.3 ± 2 m/s) (table I).

TABLE I. TEST VALUES USED IN SIMULATION OF DRAG AND SETBACK

Shot	Bird mass M1 (kg)	MEM mass M2 (kg)	Washer diam Ø (in.)	Cavity leakage area A7 (in. ²)	Initial projectile ("bird") velocity U0 (ft/s)	Bird velocity U1 (ft/s)	MEM velocity U2 (ft/s)	Mitigator
99	0.53	2.19	2.483	0.117	156	-0.6	37.9	Wood
100	0.53	2.19	2.483	0.117	160	-1.3	38.8	Wood
101	0.53	2.19	2.451	0.241	155	0.6	36.7	Wood
102	0.53	2.19	2.451	0.241	(b)	0.8 ^c	36.7 ^c	Wood
104	0.53	2.19	2.451	0.241	(b)	0.8 ^c	36.7 ^c	Wood
105	0.53	2.19	2.451	0.241	150	1.5	35.6	Wood
107	0.53	2.19	2.401	0.432	157	3.0	37.3	Wood
108	0.53	2.19	2.401	0.432	156	3.7	36.9	Wood
109	0.53	2.19	2.350	0.622	156	3.5	36.9	Wood
110	0.53	2.19	2.350	0.622	157	3.6	37.1	Wood
111	0.53	2.15	2.0	1.443	153	3.8	36.8	Wood
112	0.53	2.15	2.0	1.443	153	3.2	36.9	Wood
113	0.53	5.06	2.483	0.117	155	-3.6	16.6	Aluminum
114	0.53	5.06	2.483	0.117	154	-3.0	16.4	Aluminum
116	0.53	5.06	2.401	0.432	155	3.8	15.8	Aluminum
117	0.53	5.06	2.401	0.432	(b)	4.2	15.8 ^c	Aluminum
118	0.53	5.06	2.401	0.432	156	3.6	15.8	Aluminum
119	0.53	5.06	2.451	0.241	155	1.1	16.0	Aluminum
120	0.53	5.06	2.451	0.241	155	1.1	16.0	Aluminum
121	0.53	2.15	2.00	1.443	155	4.7	37.1	Wood
122	0.53	2.15	2.00	1.443	157	4.1	37.7	Wood
123	0.53	2.19	2.350	0.622	155	3.3	36.7	Wood
124	0.53	2.19	2.350	0.622	155	3.2	36.7	Wood
125	0.53	2.19	2.401	0.432	157	3.3	37.2	Wood
126	0.53	2.19	2.401	0.432	157	3.2	37.2	Wood

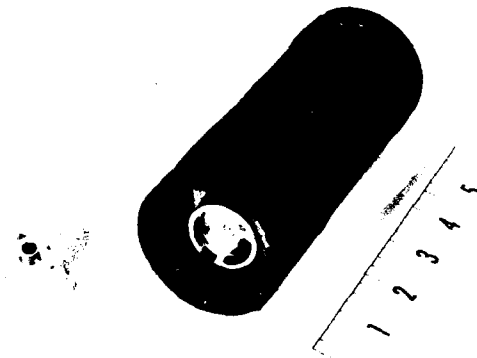
^a Includes washer weight = 40 grams.

^b No data taken.

^c Assumed value, in the absence of complete data.

To avoid any effects on drag by the air flow following the bird down the gas gun, the first contact of the bird with the mitigator occurs when the bird is completely inside the catch tube. (The gas gun and catch tube are separated by a distance of 6 in. (15 cm).) The bird setback is caused by the crushing of the mitigator, which is located just aft of the slotted opening and which is in physical contact with the MEM. Both the mitigator and the MEM are at rest prior to impact. For a nonelastic MEM (consisting only of a mass without springs), the ratio of MEM to mitigator masses is about 100, and the ratio of MEM to bird masses is about 10 for aluminum honeycomb and about 5 for wood mitigators.

The aims of the present tests were to evaluate the simulator and to simulate the setback and drag environments experienced by an arming mechanism being developed for use in Army ordnance projectiles. To this end, the bird was made of Bakelite, with a diameter of 2.483 in. (6.307 cm) at the impact section and length of 6 in. (15 cm) (fig. 3). As shown, the bird diameter aft of the impact section was reduced by 0.06 in. (0.15 cm) so that a stripe pattern attached to the bird did not make physical contact with the wall of the gas gun or catch tube. (A streak photograph of the stripes gives displacement-time data from which the bird setback and drag are obtained by double differentiation.) The interior of the bird accommodated two arming mechanisms (fig. 3).



586-76

Figure 3. Projectile ("bird") and safety and arming device.

The aluminum honeycomb mitigators had a static crush strength of 2000 psi (14 MPa); each was a cube with a 1.5-in. (3.8 cm) edge. A light plastic foam strip was taped around each aluminum mitigator to center the mitigator with the axis of the catch tube (fig. 4). The wood mitigators (four marine-grade, 3/4-in. (1.9-cm) fir plywood sections held together with masking tape) fitted snugly into the tube and were 2.9 in. (7.4 cm) long with an equilateral triangular cross section having an area of 2.0 in.² (13 cm²) (fig. 4).

Figure 4 shows the mitigators before (top) and after (bottom) impact. To attain approximately zero bird speed following a setback, the required weights of the MEM's were 2.19 kg for the wood mitigator and 5.06 kg for the aluminum honeycomb mitigator. (The MEM weights are different because the elasticity of the two mitigators is different.) The MEM's consisted of brass bars 2 in. (5 cm) in diameter with four legs at each end (fig. 5). On placing the MEM in the catch tube, the center line of each MEM was coincident with the axis of the tube.

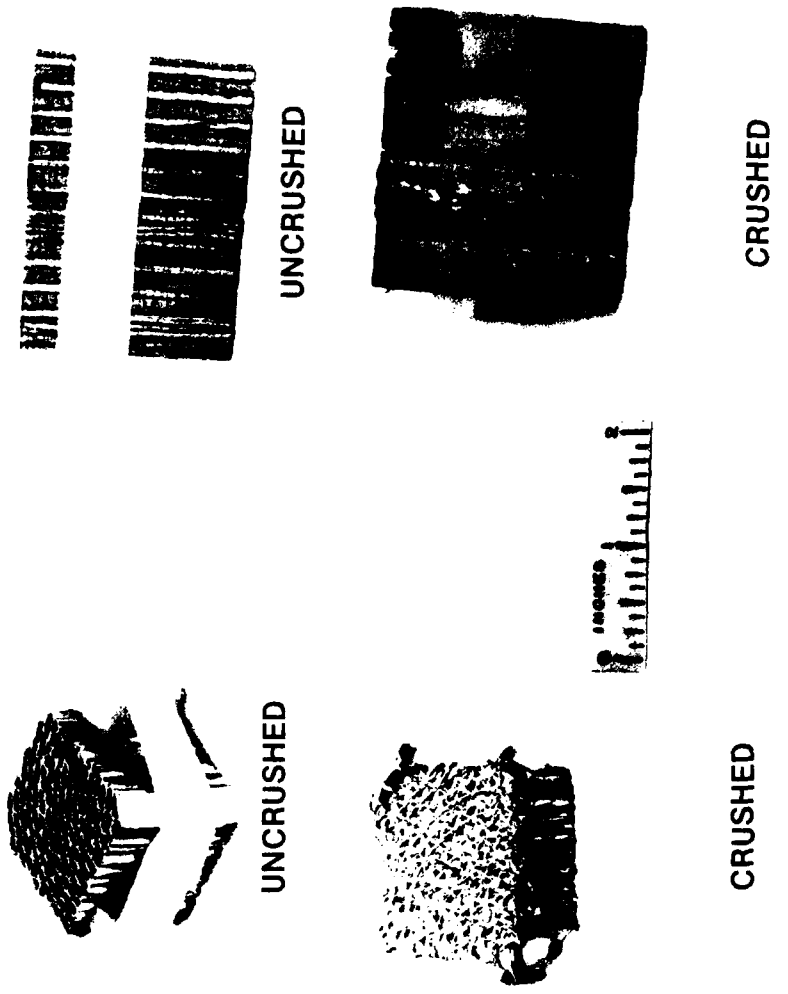
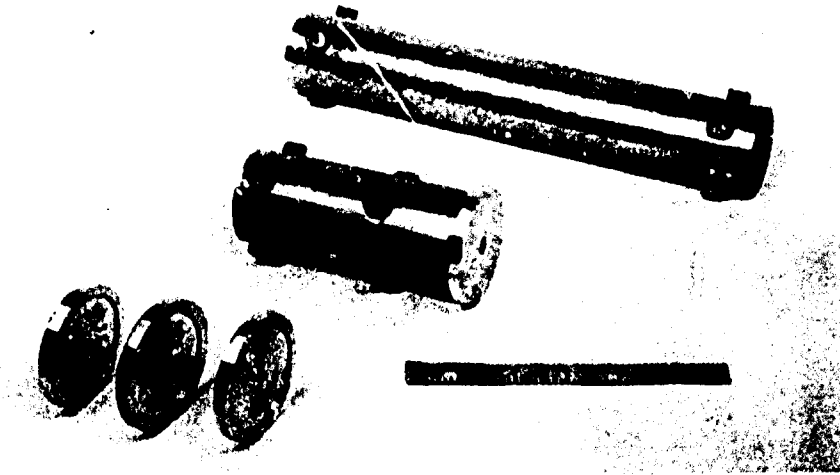


Figure 4. Aluminum honeycomb and wood mitigators.

350-76



554-76

Figure 5. Momentum exchange masses and washers.

The bird and MEM's were tested for fixed initial relative motion between the bird and the MEM following setback and for insignificant variations of cavity pressure and volume (with respect to their effect on drag). In these tests, the drag was determined by controlling the air leakage in the cavity. To control it, an aluminum washer of desired diameter was screwed to the impact end of the MEM (fig. 5). Each washer weighed about 40 grams, and the mitigator was placed in physical contact with the washer. Air leakage was determined by the size (diameter) of the washer (taking into account the small leakage past the bird into the cavity).

3. COMPUTER PROGRAMS

Computer code 1 (app A) is presented for the computation of the setback acceleration (code SETBACK for the aluminum mitigator only). The code is an adaptation of computer code VARYP case A, of Pollin.¹ Computer code 2 (app A) is presented for the computation of the acceleration caused by aerodynamic drag (code DRAG) for both aluminum and wood mitigators. Code SETBACK is based on the conservation equations for continuity, momentum, and energy. No computer code is available for wood mitigators; here, setback designs were based on unpublished HDL experimental data.

¹Irvin Pollin, *Impact Pulse Shaping, Harry Diamond Laboratories TR-1710 (June 1975)*.

The termination of the mitigator crush occurs when $U_1 = U_2$ at the time denoted by $T = T_C$. The elasticity in the mitigator produces an additional setback for a time interval at $T > T_C$. Empirical data indicate that a linear spring constant formulation yields the proper additional setback acceleration and the time at which the setback terminates. The spring constants for the aluminum and wood are based on equal displacements at each end of the mitigator of $C_1 = C_2 = 0.01$ in. (0.03 cm) for aluminum and $C_1 = C_2 = 0.06$ in. (0.15 cm) for wood at the time $T = T_C$ and for the load acting on the mitigator at that time. To facilitate the reduction of streak photograph data, the tests were designed so that the bird velocity $U_1 \approx 0$ at the termination of the setback. For this condition, the above spring constants were used in code SETBACK to determine the appropriate MEM mass for both the aluminum and the wood mitigators.

Maximum setback loading is at least 100 times larger than that for aerodynamic drag, and the setback pulse fall occurs in less than 400 μ s (fig. 6, 7). Thus, the setback and drag parts of the pulse are clearly distinguishable. The termination of the setback marks the commencement of the drag. However, because of the reduction of the cavity volume, the cavity pressure rises to about 20 psi (0.14 MPa) during the setback (sect. 4). Hence, in the computations, the commencement of drag is assumed to occur at the time during the pulse fall where the streak photograph data yield $A_1 = -22$ g (acceleration of gravity); this is the bird acceleration caused by a cavity pressure of 20 psi (0.14 MPa) in the absence of a setback. The streak photograph data give the value of U_1 at the commencement of the drag, and momentum conservation yields the corresponding value for the MEM velocity, U_2 . The measured length of the crushed mitigator is used to denote the distance separating the bird and the MEM at the commencement of drag, from which distance the corresponding volume of air in the cavity is determined.

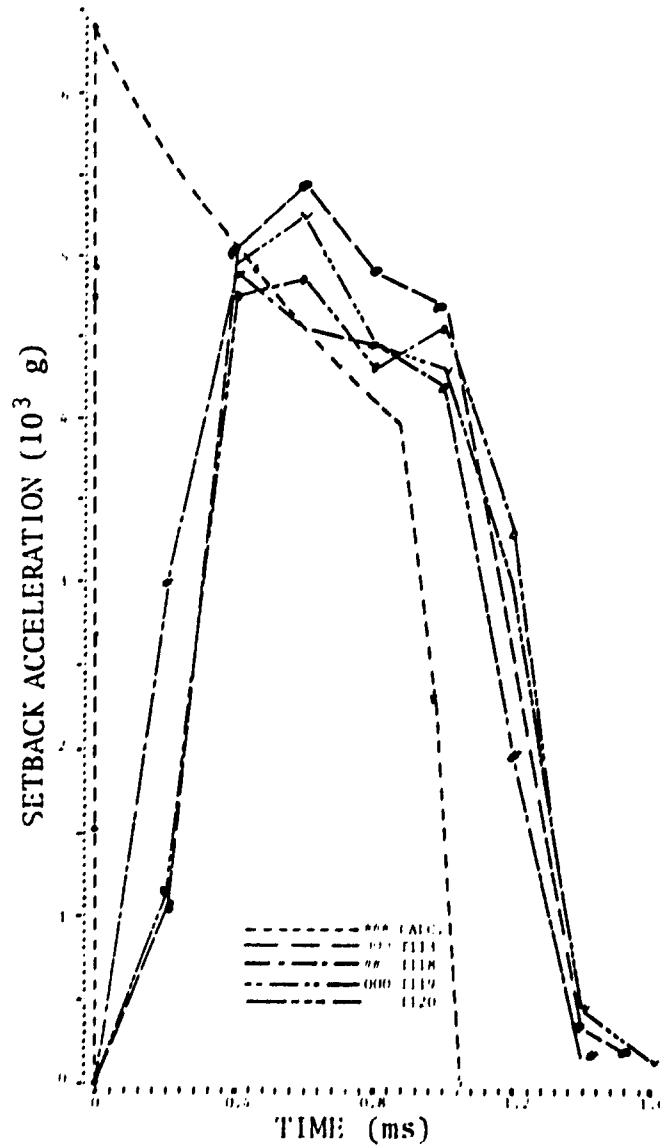


Figure 6. Calculated and experimental setback data for aluminum honeycomb mitigators (shots 113 and 118 to 120).

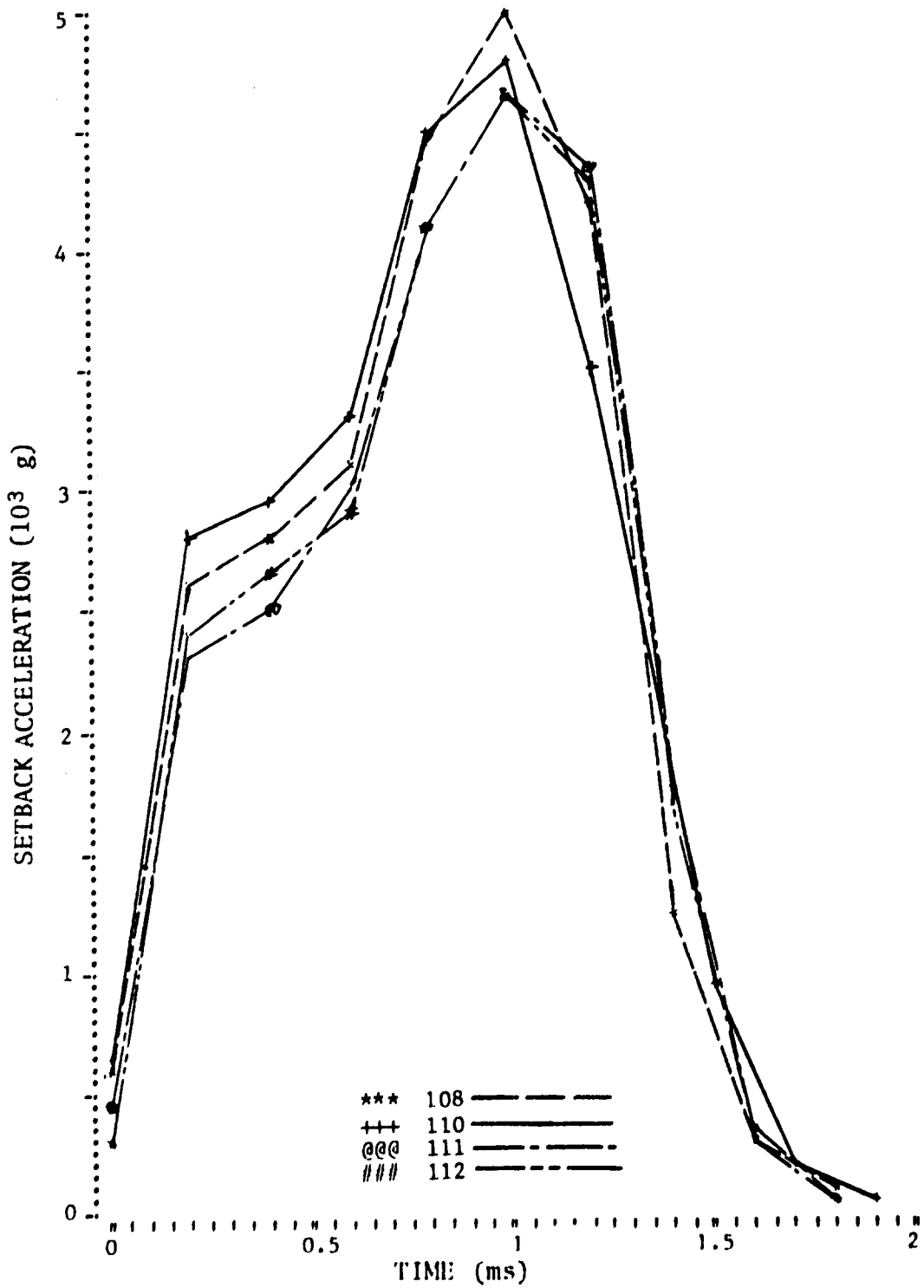


Figure 7. Experimental setback data for wood mitigators (shots 108 and 110 to 112).

3.1 Setback for Aluminum Mitigators

The impact of the bird with the mitigator (which is attached to and at rest with the MEM inside the catch tube--fig. 2) initiates crushing of the mitigator at its interface with the bird. The crush front, which is the boundary separating the crushed and uncrushed mitigator masses, proceeds toward the MEM during crushing.

The mitigator dynamic crush force is given by Pollin¹ as

$$F = 1.05AF_0[1 + 0.5(U_1 - U_2)/U_0] ,$$

where F_0 is the mitigator static crush pressure, U_1 and U_2 are instantaneous bird and MEM velocities, and U_0 is the impact bird velocity.

The hydrodynamic crush force arising from acceleration of mitigator mass at the crush front is given by

$$R = \dot{M}_4(U_1 - U_2) ,$$

where the time rate of mitigator crush (\dot{M}_4) is given by

$$\dot{M}_4 = \rho AS(U_1 - U_2) ,$$

ρ is the density of the uncrushed mitigator, A is the instantaneous crush area as measured at the bird interface, and S is the ratio of the crush front travel to the depth of the bird penetration.

The force ($F + R$) is transmitted to the mass ($M_1 + M_4$), where M_1 is the mass of the bird and M_4 is the crushed mitigator mass. Hence, the setback acceleration experienced by the bird is

$$A_1 = -(F + R)/(M_1 + M_4) .$$

¹Irvin Pollin, *Impact Pulse Shaping*, Harry Diamond Laboratories TR-1710 (June 1975).

The dynamic crush force F is transmitted to the mass $(M2 + M5)$, where $M2$ is the mass of the MEM and $M5$ is the uncrushed mitigator mass. Hence, the MEM acceleration is

$$A2 = F/(M2 + M5) \quad (2)$$

The honeycomb spring constants, $Z1$ (at the bird interface) = $Z2$ (at the MEM interface), are determined at the time $T = TC$ (time duration of the mitigator crush). They are determined by two parameters: (1) the mitigator displacements $C1 = C2 = 0.01$ in. (0.03 cm), where $C1$ and $C2$ are the mitigator elongations at the bird and MEM interfaces, and (2) the force $1.05AF0$ acting on both $M1$ and $M2$.

No elasticity is assumed for $T < TC$, and the setback ends when the forces acting on $M1$, $M2$, and $M3$ are simultaneously zero. Accordingly, for $T > TC$ to the time at which $A1 = A2 = A3 = 0$ (where $A3$ is the mitigator acceleration), the bird and MEM accelerations were computed from the equations

$$A1 = -Z1 \cdot X1/M1, \quad (3)$$

$$A2 = Z2 \cdot X2/M2, \quad (4)$$

where $X1$ is the instantaneous honeycomb elongation at the bird interface and $X2$ is that at the MEM interface.

Computed values for the bird and the MEM velocities and displacements were obtained by single and double integrations of the equations for $A1$ and $A2$.

3.2 Drag

The drag force is determined entirely by the cavity and the ambient atmospheric pressures acting on the bird face. For the reasons discussed in section 4, it is sufficient to assume that the initial volume for the air in the cavity was 4.92 in.³ (80.6 cm³) and the initial cavity air pressure was 20 psi (0.14 MPa) for all test conditions. Table I shows the initial bird and MEM speeds for each test. The cavity pressure changes as a result of the air leakage into or out of the cavity and as a result of the change of the cavity volume arising from the relative motion between the bird and the MEM. Incompressible air flow is assumed at a temperature of $530^\circ R$, and the leakage velocity $U7$ is computed from the equation

$$U7 = C(2|P0 - P|/D7)^{1/2} \quad (5)$$

where the friction coefficient $C = 0.5$ for incompressible air flow with friction and $C = 1.0$ for Bernoulli (frictionless) incompressible air flow, $P0$ is the ambient atmospheric pressure, P is the total air pressure in the cavity, and $D7$ is the air density. The actual air leakage can be expected to have a value of C in the range $0.5 < C < 1$. The mass rate of flow into or out of the cavity is given by

$$R7 = D7 \cdot U7 \cdot A7$$

The cavity pressure is the sum of the partial pressures of the initial air in the cavity and the air leakage. Code DRAG computes the above quantities at small time intervals during the aerodynamic drag phase.

4. THEORETICAL AND EXPERIMENTAL RESULTS

Table I summarizes the tests that were run for the setback and the drag for the two types of mitigators and for the washer diameters of 2.483, 2.451, 2.401, and 2.350 in. (6.307, 6.226, 6.099, and 5.969 cm). Tests were run also without any washers, so that the obstructed area was that of the MEM cross section. The MEM has a diameter of 2.000 in. (5.080 cm), to which must be added the projected area 0.375 in.^2 (2.42 cm^2) of the four legs at each end of the MEM. The catch tube diameter measured 2.503 in. (6.358 cm) and the bird diameter measured 2.483 in. (6.307 cm), which resulted in a leakage area of 0.0783 in.^2 (0.505 cm^2). Area $A7$ is the sum of the leakage areas about the bird and washer/MEM into the cavity. The table also gives the streak photograph values for $U0$ and $U1$ and the values for $U2$ computed from momentum conservation. Both $U1$ and $U2$ are for the time denoting the termination of setback.

4.1 Setback

The streak camera was run at a comparatively slow speed so that both the setback and the drag could be recorded on a single photograph. The photograph covered a period of 20 ms, of which only about 1.5 ms consisted of the setback. The setback displacement-time data were taken at 200- μ s intervals. These time intervals are large compared with the setback pulse duration, so that the reduced data "smooths" the actual pulse shape. Notably, the rise and fall times are lengthened and the $A1_{\text{max}}$ is decreased.

Figure 6 shows the reduced experimental setback data of four typical tests for Al with aluminum honeycomb mitigators. If one allows for an uncertainty (shift of the time axis) of 50 μ s in determining the beginning of the test pulse, the differences between experimental data are generally within about 10 percent of the average value of the Al data for the given time. Figure 6 shows also the calculated values for Al based on the work of Pollin.¹ The calculated and experimental data can be brought into good agreement, recalling that the experimental displacement data are read at 200- μ s intervals.

Figure 7 shows typical experimental setback pulses with wood mitigators. The wood and aluminum mitigators yielded approximately equal peak accelerations, although the wood gave longer pulse duration. Having the same value for UO and approximately zero terminal velocity, the two sets of pulses have the same area under the curve since

$$UO = \int_0^{TS} A_l dt ,$$

where T = TS is the time of the setback pulse. The pulse time is larger for the wood mitigator because its curve is less rectangular. The test-to-test repeatability of Al for the wood mitigators is about the same as that noted above for the aluminum.

A reliable measure of this test data precision (which differs from that for drag) is given by the fluctuation of the data during the free-flight bird travel over a distance of approximately 1.5 in. (3.8 cm) before the setback begins. Accordingly, the average random error in determining the setback velocity and acceleration were found to be 1 ft/s (0.3 m/s) and 200 g.

4.2 Drag

The bird velocity is generally less than 10 ft/s (3.0 m/s) during the entire drag phase. To determine the measurement precision, three streak photographs were obtained with the bird at rest. (That is, the bird was inserted into the slotted opening of the catch tube--which is in the camera field of view, and three streak photographs were taken with the bird at rest in the same way as for an actual test for the setback or the drag.) The test data precision is given by the fluctuation of the data for this condition. The average random error in determining velocity and acceleration during the drag phase was found to be 0.1 ft/s (0.03 m/s) and 1 g. A few measurements were found to be in error by 2 g, and one error amounted to 3 g. The timewise

¹Irvin Pollin, *Impact Pulse Shaping*, Harry Diamond Laboratories TR-1710 (June 1975).

point-by-point fluctuation of the drag acceleration with the bird at rest is shown in figure 8. Although test data of bird displacement were taken at time intervals of 400 μ s, calculations for the acceleration were made at intervals of 800 μ s. The test data shown in figure 8 are separated at 400- μ s intervals. This difference results from the fact that two overlapping sets of data points at 800- μ s time intervals, separated by 400 μ s, were prepared from each photograph.

On the average, the wood and aluminum mitigators were each crushed 0.7 in. (2 cm). The variation of crush above or below 0.7 in. (2 cm) was within 5 percent. This is consistent with the previously noted <10-percent variation of the setback acceleration. The initial bird impact with the mitigator occurred 0.25 in. (0.64 cm) aft of the slotted opening of the catch tube. Starting from the bird position at the edge of the slotted opening, the volume of air in the cavity was 9.99 in.³ (164 cm³) for the wood mitigator and 5.44 in.³ (89.1 cm³) for the aluminum mitigator. At the termination of the setback, the air volumes were 6.40 in.³ (105 cm³) for the wood mitigator and 3.48 in.³ (57.0 cm³) for the aluminum mitigator. Thus, for both mitigators, the compression ratio was 1.56. Assuming isentropic or isothermal compression without leakage, the corresponding cavity air pressure was 27.4 or 22.9 psi (0.189 or 0.158 MPa). However, up to the termination of the setback, there was a time interval of about 1.5 ms for leakage to occur, and the corresponding amount of the reduction of the cavity pressure depended on A7. We can assume a cavity volume of 4.92 in.³ (80.6 cm³) so that, in the absence of the mitigator, the length of the cavity at the termination of the setback $L_0 = 1$ in. (2.5 cm). Table II(A) shows the drag induced $A_1(T)$ for incompressible frictionless flow with cavity pressures at the beginning of the drag of 20 and 30 psi (0.14 and 0.21 MPa) for A7 values of 0.117 and 1.068 in.² (0.755 and 6.890 cm²). There is a small effect of cavity pressure on A_1 up to about 5 ms for $A_7 = 0.117$ in.² (0.755 cm²) and negligible effect on A_1 beyond 1 ms for $A_7 = 1.068$ in.² (6.890 cm²). The net time effect is further reduced if we take into account the time required for the setback.

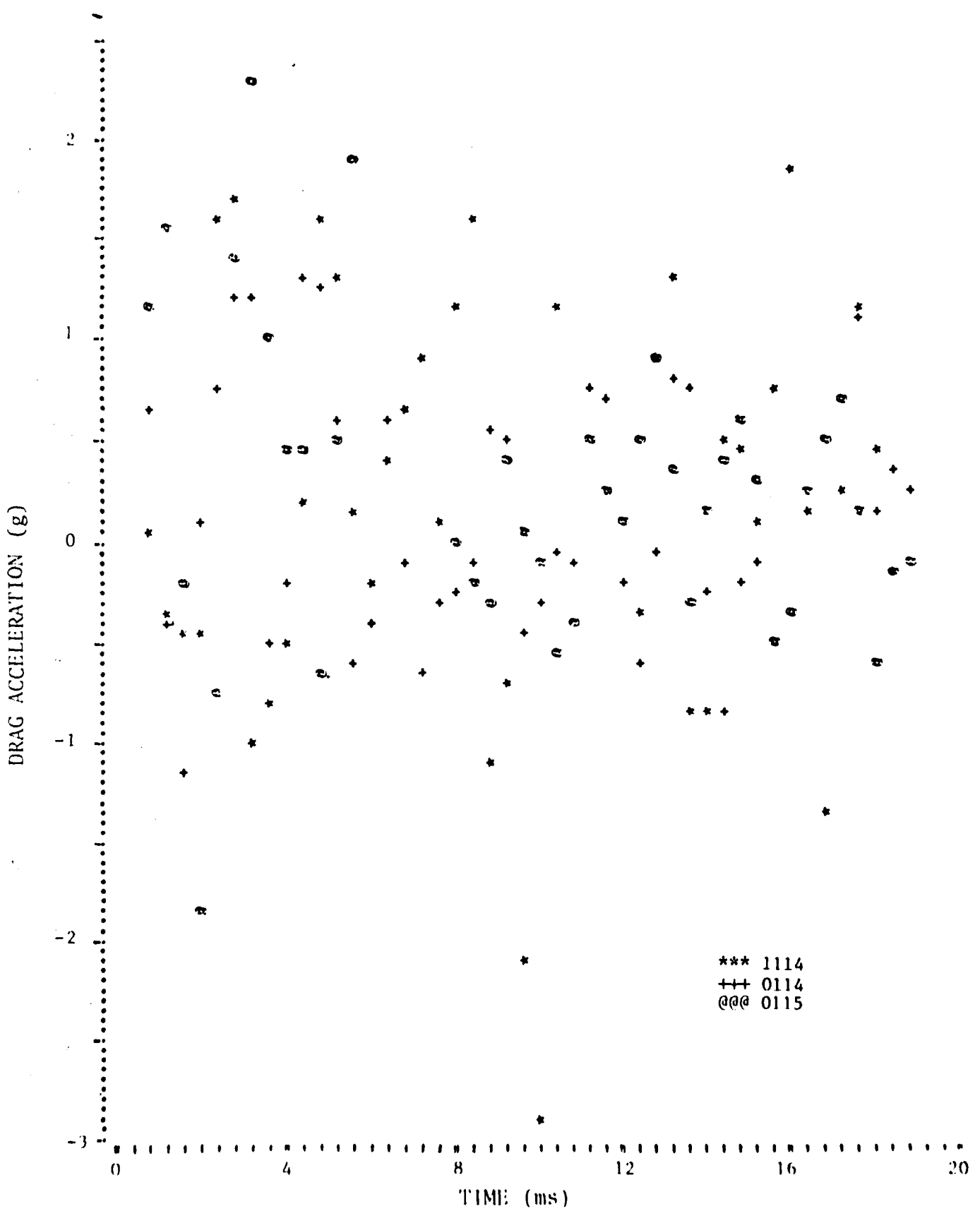


Figure 8. Precision of drag measurements.

TABLE II. EFFECTS OF INITIAL CAVITY PRESSURE AND VOLUME ON AERODYNAMIC DRAG

(A) Effects of Initial Cavity Pressure

LO=	P=	A/=	C=	1,	30,	117,	1								
TIME	A1	U1	Y1	A2	U2	Y2	M1	M2	U1	P					
0.	.70	3.4	.00	.00	36.9	.00	.00	.00	.0	.0	30.0				
1.	-16.20	2.2	.03	3.43	37.2	.45	-.07	-3.3	317.3	13.6					
2.	4.46	2.1	.00	-1.06	37.2	.89	-.08	-1.1	317.9	13.6					
3.	11.48	2.4	.04	-2.71	37.1	1.34	-.05	-1.0	508.8	12.0					
4.	15.19	2.9	.12	-3.59	37.0	1.74	-.01	-.3	662.6	11.1					
5.	17.40	3.4	.15	-4.11	36.9	2.23	.03	.7	112.5	10.6					
6.	18.79	4.0	.20	-4.44	36.9	2.67	.07	1.5	741.9	10.2					
7.	19.69	4.6	.25	-4.65	36.6	3.11	.12	2.2	760.3	11.0					
8.	20.27	5.2	.31	-4.79	36.5	3.55	.17	2.7	111.9	9.9					
9.	20.65	6.0	.33	-4.83	36.3	4.03	.22	3.3	119.7	9.8					
10.	20.93	6.0	.45	-4.92	36.7	4.42	.26	3.7	763.3	9.7					

LO=	P=	A/=	C=	1,	20,	117,	1								
TIME	A1	U1	Y1	A2	U2	Y2	M1	M2	U1	P					
0.	.70	3.4	.00	.00	36.9	.00	.00	.00	.0	.0	20.0				
1.	4.77	3.2	.04	-1.13	36.9	.44	-.02	-1.1	319.7	13.6					
2.	12.69	3.5	.08	-3.00	36.9	.89	.01	.4	599.7	11.7					
3.	16.35	4.0	.12	-3.86	36.9	1.33	.05	1.0	673.4	10.8					
4.	18.33	4.6	.14	-4.33	36.6	1.77	.09	2.5	731.9	10.3					
5.	19.47	5.2	.24	-4.60	36.5	2.21	.14	3.3	755.7	10.1					
6.	20.14	5.8	.30	-4.76	36.3	2.64	.18	3.9	669.3	9.9					
7.	20.51	6.5	.38	-4.85	36.2	3.09	.23	4.4	716.9	9.8					
8.	20.70	7.1	.45	-4.89	36.0	3.51	.28	4.9	767.7	9.8					
9.	20.75	7.9	.50	-4.97	35.3	3.99	.33	5.2	761.9	9.8					
10.	20.71	8.5	.65	-4.89	35.7	4.37	.37	5.5	761.3	9.8					

LO=	P=	A/=	C=	1,	30,	1.064,	1								
TIME	A1	U1	Y1	A2	U2	Y2	M1	M2	U1	P					
0.	.70	3.4	.00	.00	36.9	.00	.00	.00	.0	.0	30.0				
1.	.79	3.2	.04	-.15	36.9	.44	-.15	-1.5	153.0	14.5					
2.	.79	3.2	.08	-.15	36.9	.89	-.05	-2.4	152.0	14.5					
3.	.79	3.3	.12	-.15	36.9	1.33	.02	.7	152.7	14.5					
4.	.79	3.3	.16	-.15	36.9	1.77	.11	2.9	159.6	14.5					
5.	.79	3.3	.19	-.15	36.9	2.22	.19	4.4	152.5	14.5					
6.	.79	3.3	.23	-.15	36.9	2.66	.24	5.6	152.4	14.5					
7.	.79	3.4	.27	-.15	36.9	3.10	.35	6.6	152.2	14.5					
8.	.78	3.4	.31	-.15	36.9	3.54	.45	7.4	152.1	14.5					
9.	.78	3.4	.36	-.15	36.9	4.03	.54	8.0	152.0	14.5					
10.	.78	3.4	.40	-.15	36.9	4.43	.61	8.5	151.9	14.5					

LO=	P=	A/=	C=	1,	20,	1.064,	1								
TIME	A1	U1	Y1	A2	U2	Y2	M1	M2	U1	P					
0.	.70	3.4	.00	.00	36.9	.00	.00	.00	.0	.0	20.0				
1.	.78	3.4	.04	-.15	36.9	.44	-.00	-.2	152.0	14.5					
2.	.78	3.4	.08	-.15	36.9	.89	.04	3.2	151.9	14.5					
3.	.78	3.4	.12	-.15	36.9	1.33	.17	5.3	151.7	14.5					
4.	.78	3.5	.16	-.15	36.9	1.77	.25	6.7	151.6	14.5					
5.	.78	3.5	.21	-.15	36.9	2.21	.33	7.8	151.5	14.5					
6.	.78	3.5	.25	-.15	36.9	2.66	.42	8.6	151.3	14.5					
7.	.78	3.5	.29	-.15	36.9	3.10	.50	9.2	151.2	14.5					
8.	.77	3.6	.33	-.15	36.9	3.54	.59	9.7	151.1	14.5					
9.	.77	3.6	.38	-.15	36.9	4.03	.64	10.2	150.9	14.5					
10.	.77	3.6	.42	-.15	36.9	4.43	.75	10.5	150.8	14.5					

NOTE: (M1 = 0.53, M2 = 2.19, U1 = 3.4, and U2 = 36.9)

TABLE II. EFFECTS OF INITIAL CAVITY PRESSURE AND VOLUME ON AERODYNAMIC DRAG (Cont'd)

(B) Effects of Initial Cavity Volume

LO=1	P=1	A7=1	C=7	1.3,20,117,1								
TIME	A1	U1	Y1	A2	U2	Y2	M1	M2	U1	P		
0.	.00	3.4	.00	.00	36.9	.00	.70	.0	.7	20.0		
1.	1.51	3.1	.04	-.36	37.0	.44	-.03	-1.3	1.3	14.3		
2.	9.86	3.3	.08	-2.33	36.9	.89	-.01	-.2	522.9	12.4		
3.	14.03	3.7	.12	-3.31	36.8	1.33	.03	.8	635.7	11.4		
4.	16.46	4.2	.17	-3.89	36.7	1.77	.07	1.7	692.4	10.8		
5.	17.97	4.8	.22	-4.25	36.6	2.21	.11	2.4	725.2	10.4		
6.	18.93	5.4	.28	-4.47	36.4	2.65	.16	3.0	745.4	10.2		
7.	19.55	6.0	.35	-4.62	36.3	3.08	.20	3.5	758.1	10.0		
8.	19.94	6.7	.43	-4.71	36.1	3.52	.25	4.0	765.9	10.0		
9.	20.17	7.4	.52	-4.77	36.0	3.99	.30	4.4	770.7	9.9		
10.	20.26	8.0	.60	-4.79	35.8	4.38	.34	4.7	772.5	9.9		

LO=1	P=1	A7=1	C=7	.7,20,117,1								
TIME	A1	U1	Y1	A2	U2	Y2	M1	M2	U1	P		
0.	.00	3.4	.00	.00	36.9	.00	.00	.0	.7	20.0		
1.	9.07	3.3	.04	-2.14	36.9	.44	-.01	-.6	460.3	12.5		
2.	16.08	3.6	.08	-3.80	36.8	.89	.03	1.3	619.2	10.9		
3.	18.90	4.4	.13	-4.47	36.7	1.33	.07	2.7	742.5	10.2		
4.	20.25	5.0	.19	-4.78	36.5	1.77	.12	3.6	770.7	9.9		
5.	20.92	5.7	.25	-4.94	36.4	2.20	.16	4.4	784.4	9.7		
6.	21.24	6.3	.32	-5.02	36.2	2.64	.21	4.9	790.7	9.6		
7.	21.34	7.0	.41	-5.04	36.0	3.07	.26	5.4	793.0	9.6		
8.	21.31	7.7	.49	-5.03	35.9	3.50	.31	5.8	792.5	9.6		
9.	21.17	8.5	.60	-5.00	35.7	3.98	.36	6.2	790.1	9.7		
10.	21.00	9.1	.70	-4.96	35.6	4.36	.41	6.5	787.0	9.7		

LO=1	P=1	A7=1	C=7	1.3,20,1.064,1								
TIME	A1	U1	Y1	A2	U2	Y2	M1	M2	U1	P		
0.	.00	3.4	.00	.00	36.9	.00	.70	.0	.7	20.0		
1.	.78	3.4	.04	-.15	36.9	.44	-.03	-1.1	152.1	14.5		
2.	.78	3.4	.08	-.15	36.9	.89	.06	1.9	152.7	14.5		
3.	.78	3.4	.12	-.15	36.9	1.33	.14	4.0	151.5	14.5		
4.	.78	3.5	.16	-.15	36.9	1.77	.23	5.4	151.7	14.5		
5.	.78	3.5	.21	-.15	36.9	2.21	.31	6.6	151.6	14.5		
6.	.78	3.5	.25	-.15	36.9	2.66	.39	7.4	151.4	14.5		
7.	.78	3.5	.29	-.15	36.9	3.10	.48	8.1	151.3	14.5		
8.	.76	3.6	.33	-.15	36.9	3.54	.56	8.7	151.2	14.5		
9.	.77	3.6	.38	-.15	36.9	4.03	.65	9.2	151.0	14.5		
10.	.77	3.6	.42	-.15	36.9	4.43	.73	9.6	150.9	14.5		

LO=1	P=1	A7=1	C=7	.7,20,1.064,1								
TIME	A1	U1	Y1	A2	U2	Y2	M1	M2	U1	P		
0.	.00	3.4	.00	.00	36.9	.00	.70	.0	.7	20.0		
1.	.81	3.4	.04	-.15	36.9	.44	.02	1.3	145.8	14.5		
2.	.78	3.5	.08	-.15	36.9	.89	.10	4.9	151.7	14.5		
3.	.78	3.5	.12	-.15	36.9	1.33	.19	7.0	151.5	14.5		
4.	.78	3.5	.17	-.15	36.9	1.77	.27	8.3	151.4	14.5		
5.	.78	3.5	.21	-.15	36.9	2.21	.36	9.3	151.3	14.5		
6.	.78	3.6	.25	-.15	36.9	2.66	.44	9.9	151.2	14.5		
7.	.77	3.6	.29	-.15	36.9	3.10	.52	10.5	151.0	14.5		
8.	.77	3.6	.34	-.15	36.9	3.54	.61	10.9	150.9	14.5		
9.	.77	3.6	.38	-.15	36.9	4.03	.70	11.3	150.8	14.5		
10.	.77	3.7	.42	-.15	36.9	4.42	.78	11.5	150.6	14.5		

NOTE: (M1 = 0.53, M2 = 2.19, U1 = 3.4, and U2 = 36.9)

The cavity volumes at the beginning of the drag for the wood and aluminum mitigators were 1.3 and 0.7 times larger than the volume 4.92 in.^3 (79.5 cm^3). If one assumes an initial cavity air pressure of 20 psi (0.14 MPa), table II(B) gives the drag induced $A_1(T)$ for incompressible frictionless flow with LO values of 1.3 in. (3.3 cm) and 0.7 in. (2 cm) (corresponding values of LO for the above volumes) and for A7 equal to 0.117 and 1.068 in.² (0.755 and 6.890 cm^2). The effect of initial cavity volume on A_1 is approximately the same as that found above for initial cavity pressure.

In the following comparison between the predicted and experimental drag acceleration data (fig. 9 to 16), the initial cavity air pressure and volume were taken as 20 psi (0.14 MPa) and 4.92 in.^3 (79.5 cm^3). The calculated values (solid lines) are given for frictional and frictionless ($C = 0.5$ and $C = 1.0$) incompressible air flow into the cavity. In every figure, the calculated drag for the frictional flow (denoted by *) is larger than the comparable frictionless flow (denoted by +), because friction slows the flow into the cavity. In turn, this decrease reduces cavity pressure (and thereby increases drag) because of the cavity volume increase arising from the motion of the MEM relative to the bird. Similarly, reduced A7 yields larger drag.

For all values of A7 and for both wood and aluminum mitigators at the termination of the setback (that is, when the force acting on the bird due to the mitigator was relaxed to zero), the cavity pressure exceeded that of the ambient atmosphere, and the aerodynamic drag force was in the same direction as that for a setback. However, the expansion of the cavity volume very quickly led to reduced cavity pressure, and the drag force changed direction. As shown in figures 9 to 16 and table II, the experimental data (individual shot numbers are denoted by the prescript letter T) and the calculated data (denoted by the prescript letter C) show that a state of steady drag occurred within about 4 ms. Drag accelerations up to 30 g were obtained. For equal values of A7, the wood mitigators yielded larger drags than that for aluminum because of the higher elasticity of wood mitigators and the resulting larger relative speeds between the MEM and the bird.

If one allows for the previously noted measurement precision, the experimental data are in good agreement with the predicted data for a frictional incompressible flow with values of C in the range of $0.5 < C < 1.0$. For each mitigator, the experimental data indicate that the value of C is nearly 1 for the larger A7 and reduces with decreasing A7. This reduction would agree with the higher flow velocities through a smaller gap and thereby higher shear stresses associated with the smaller leakage rates.

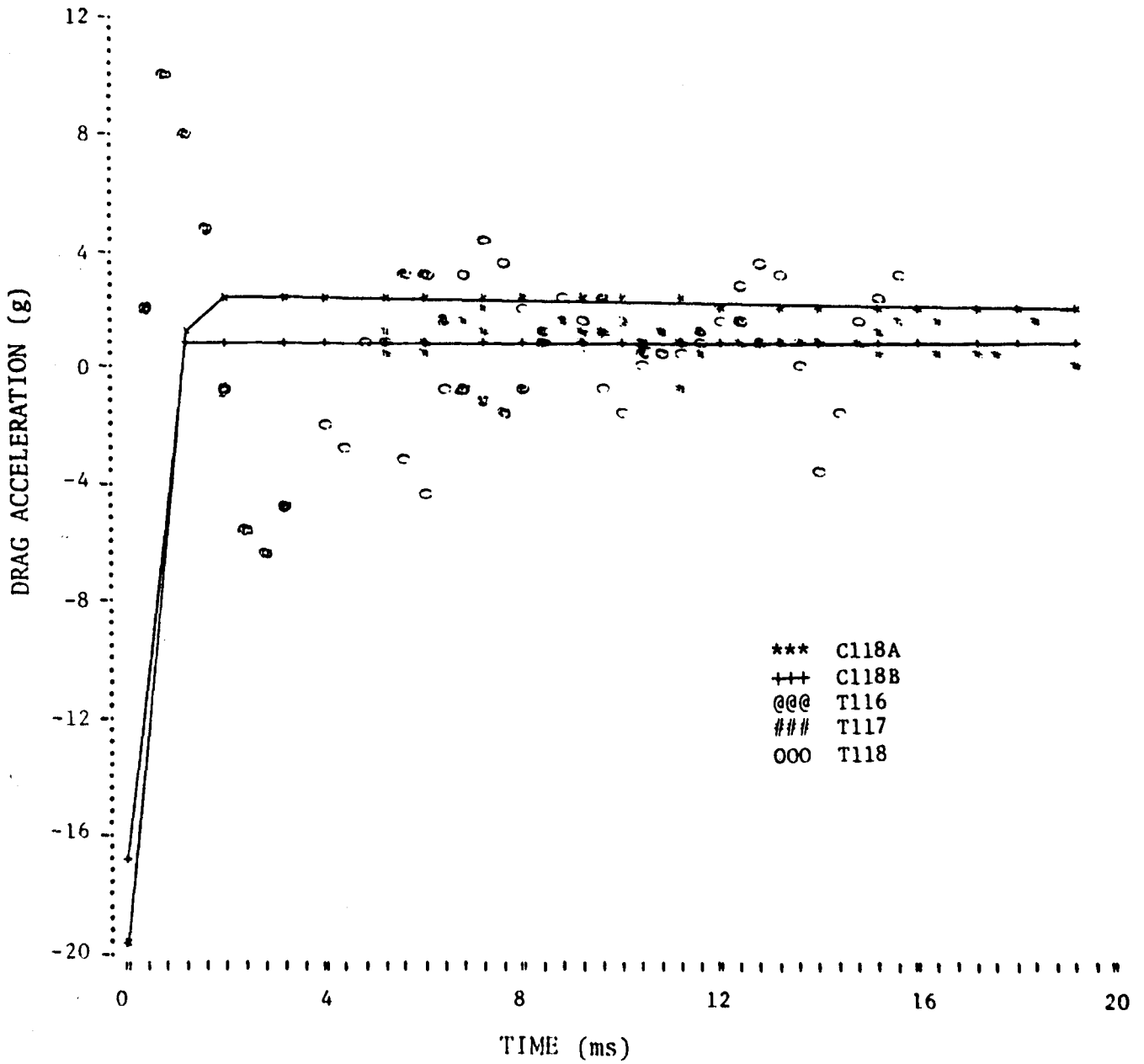


Figure 9. Calculated and experimental drag data for aluminum honeycomb mitigator ($A_7 = 0.432 \text{ in.}^2$; shots 116 to 118).

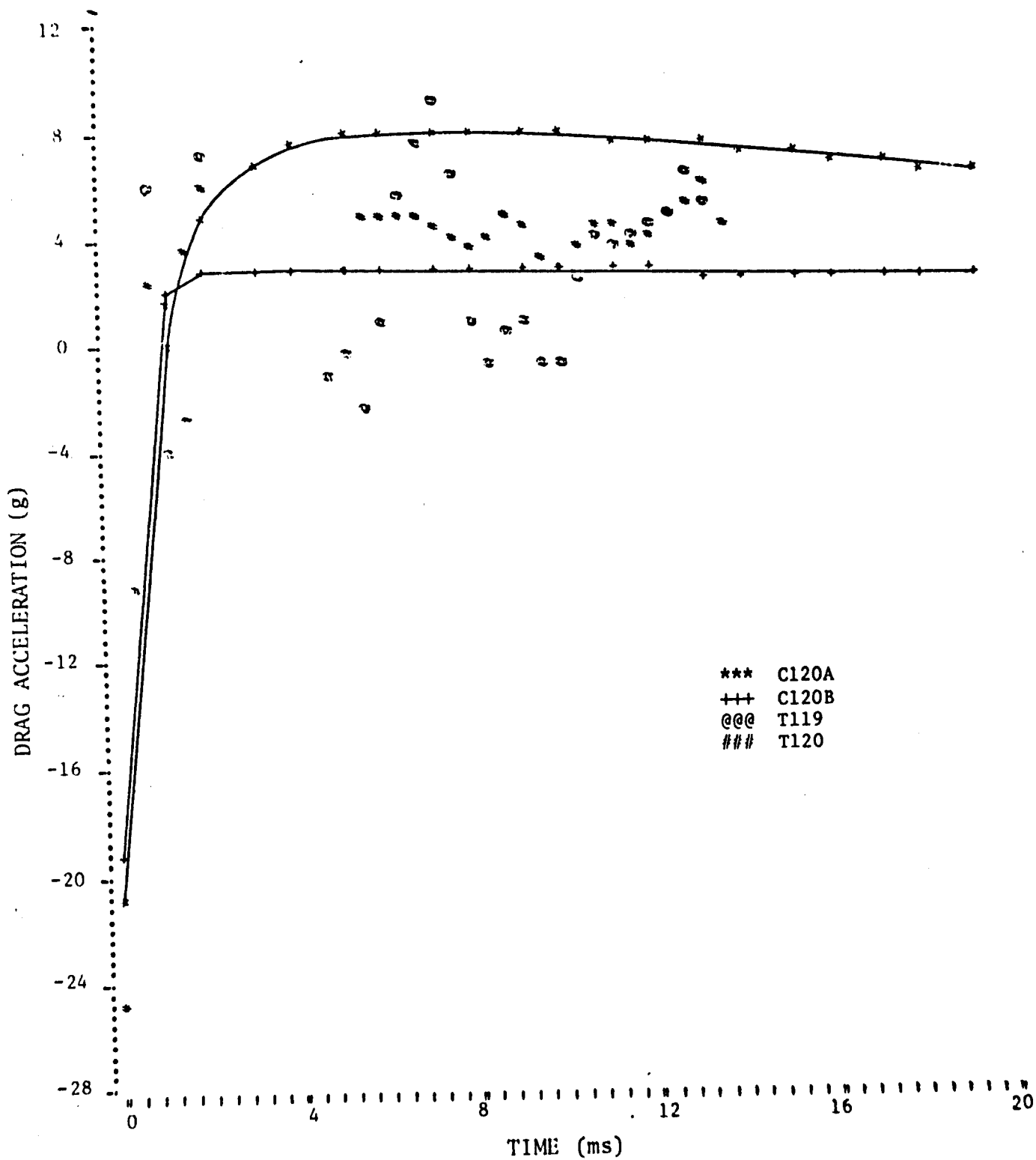


Figure 10. Calculated and experimental drag data for aluminum honeycomb mitigator ($A_7 = 0.241 \text{ in.}^2$; shots 119 and 120).

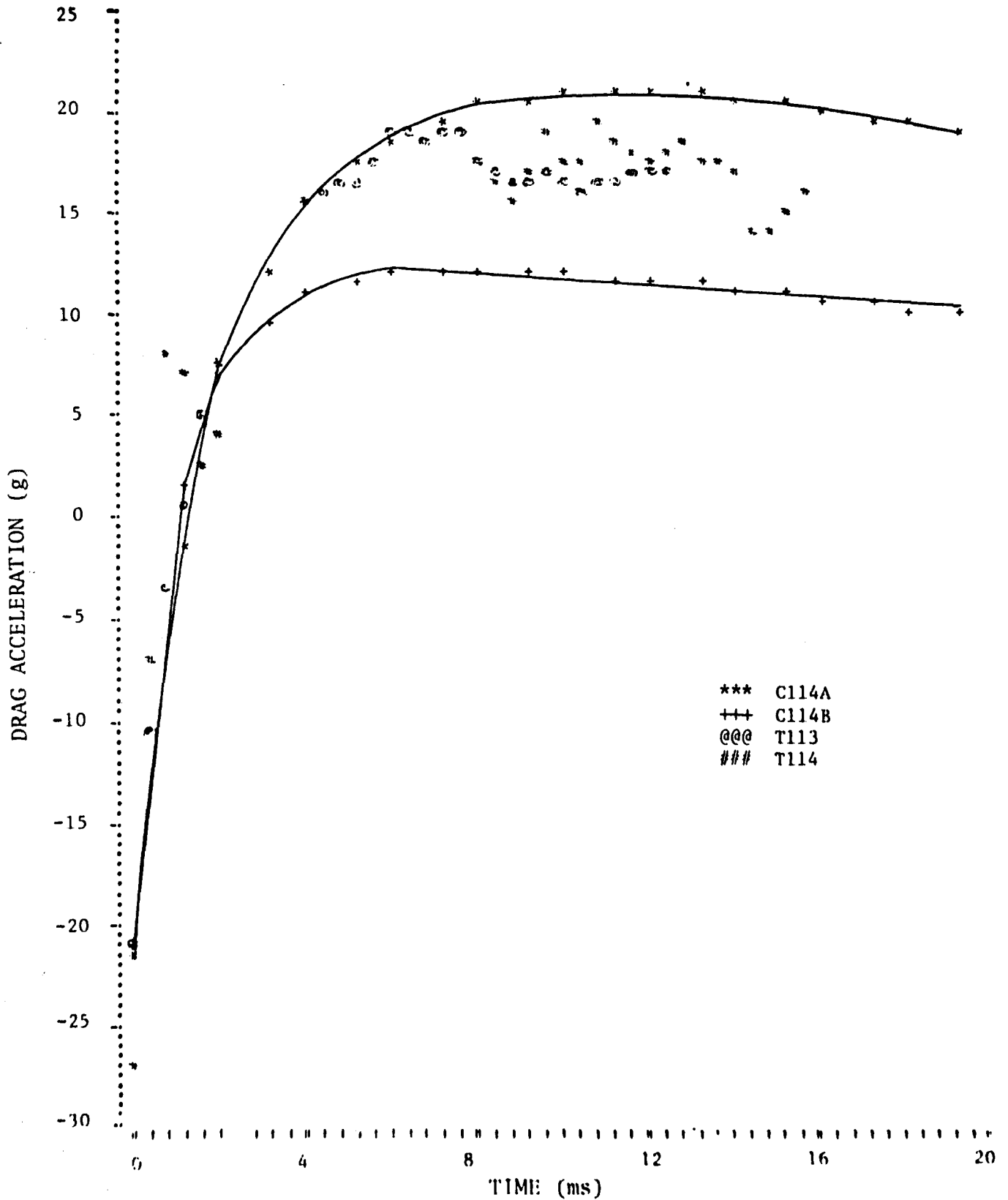


Figure 11. Calculated and experimental drag data for aluminum honeycomb mitigator ($A7 = 0.117 \text{ in.}^2$; shots 113 and 114).

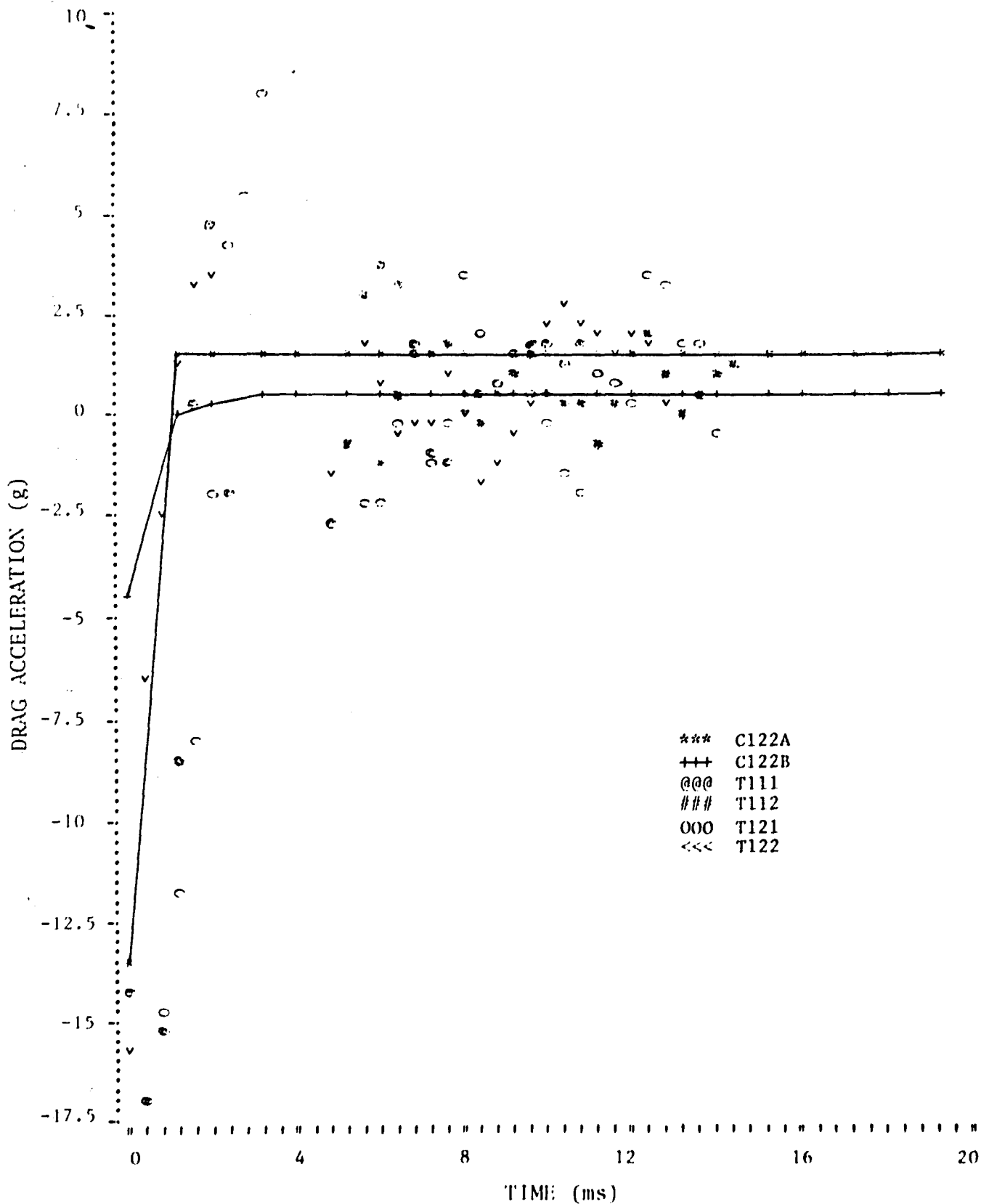


Figure 12. Calculated and experimental drag data for wood mitigator ($A7 = 1.443 \text{ in.}^2$; shots 111, 112, 121, and 122).

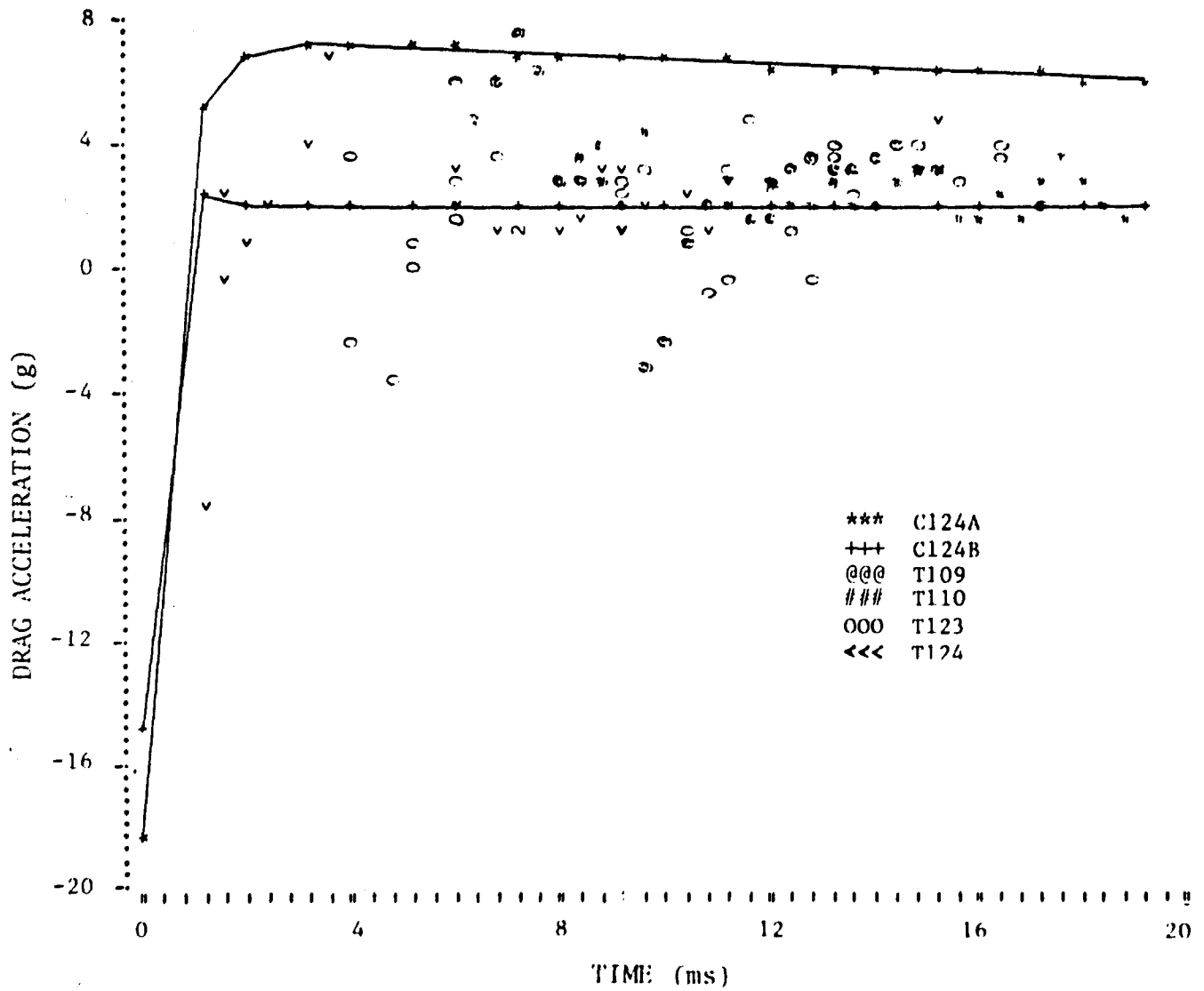


Figure 13. Calculated and experimental drag data for wood mitigator ($A_7 = 0.622 \text{ in.}^2$; shots 109, 110, 123, and 124).

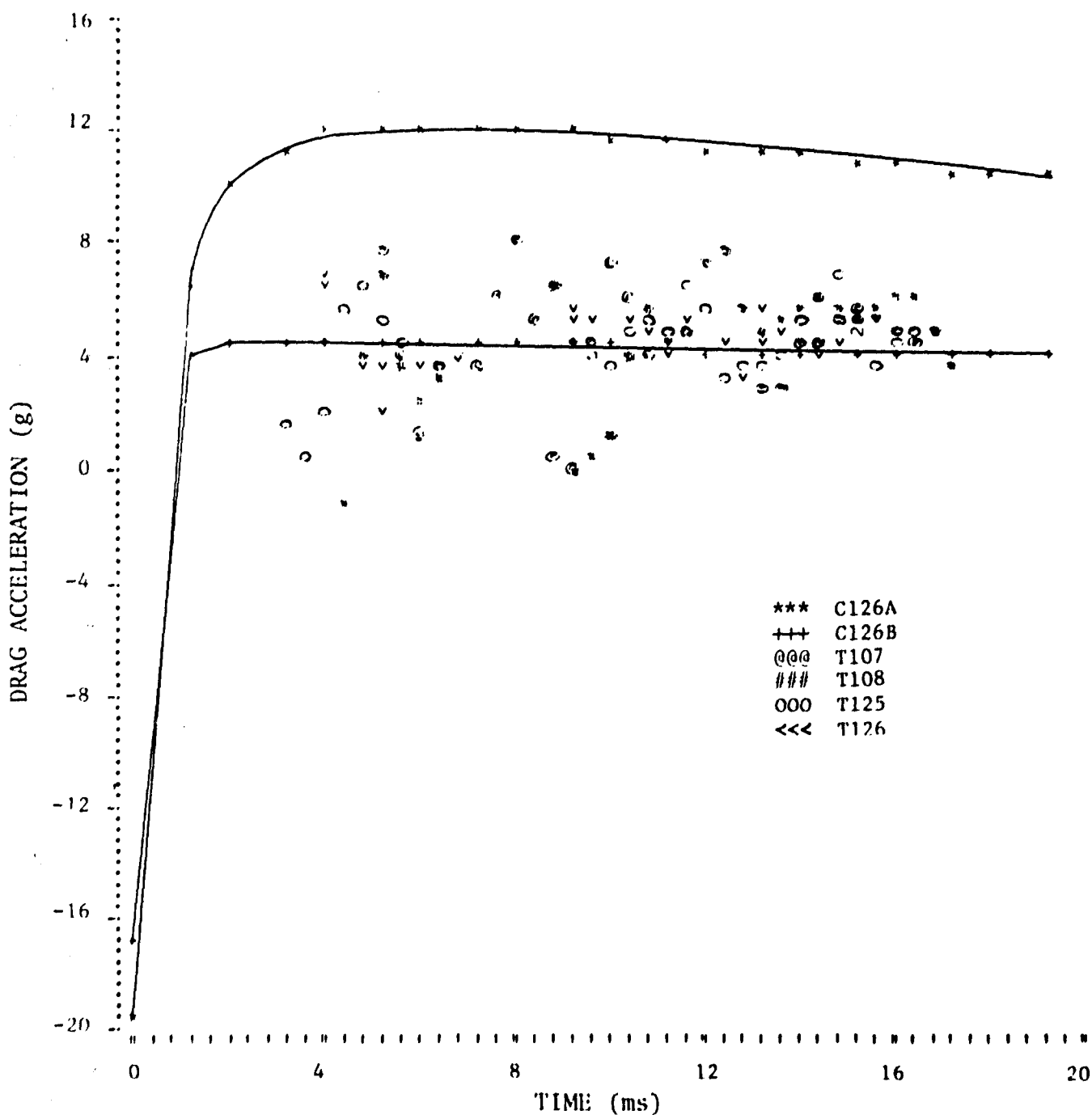


Figure 14. Calculated and experimental drag data for wood mitigator ($A_7 = 0.432 \text{ in.}^2$; shots 107, 108, 125, and 126).

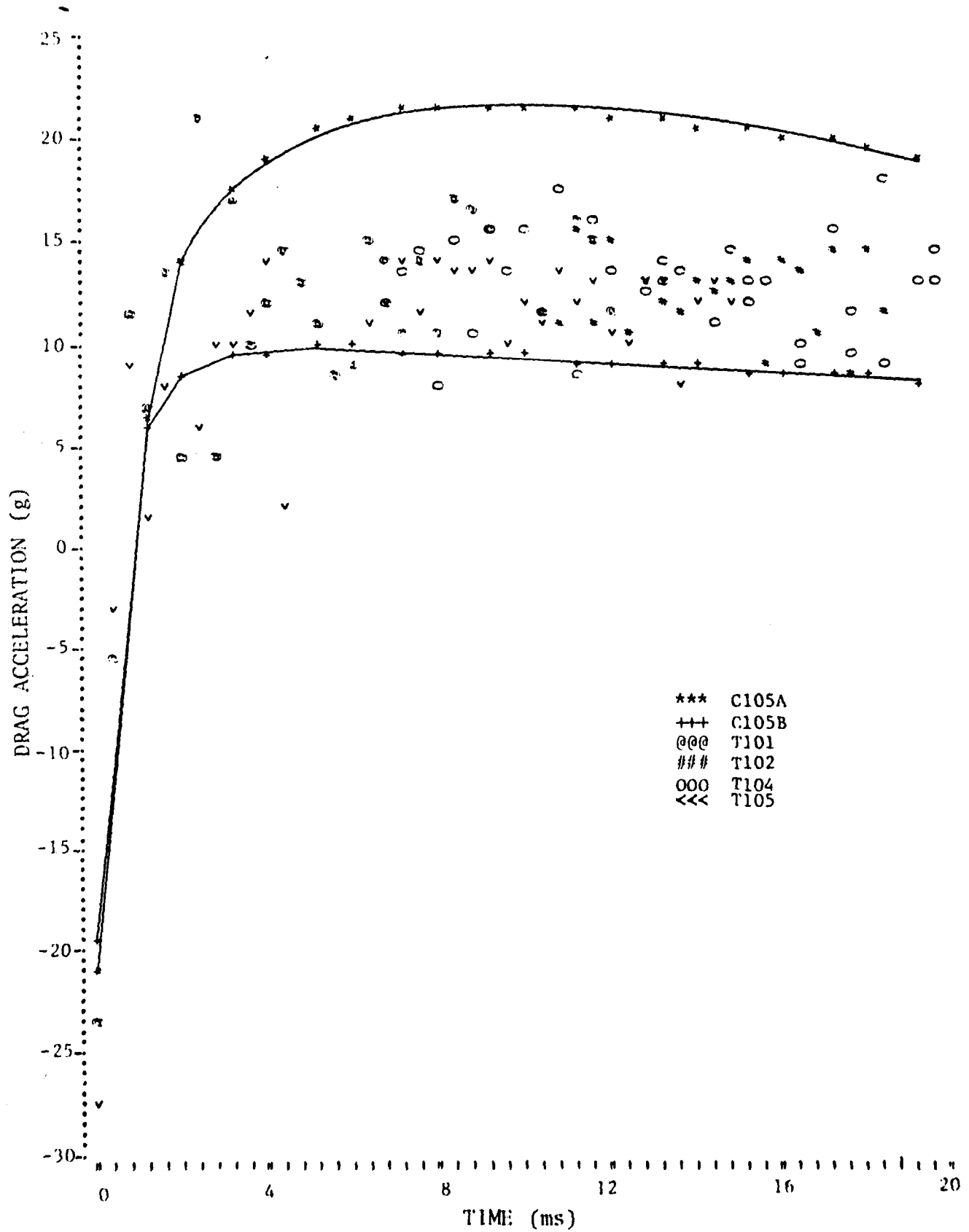


Figure 15. Calculated and experimental drag data for wood mitigator ($A7 = 0.241 \text{ in.}^2$; shots 101, 102, 104, and 105).

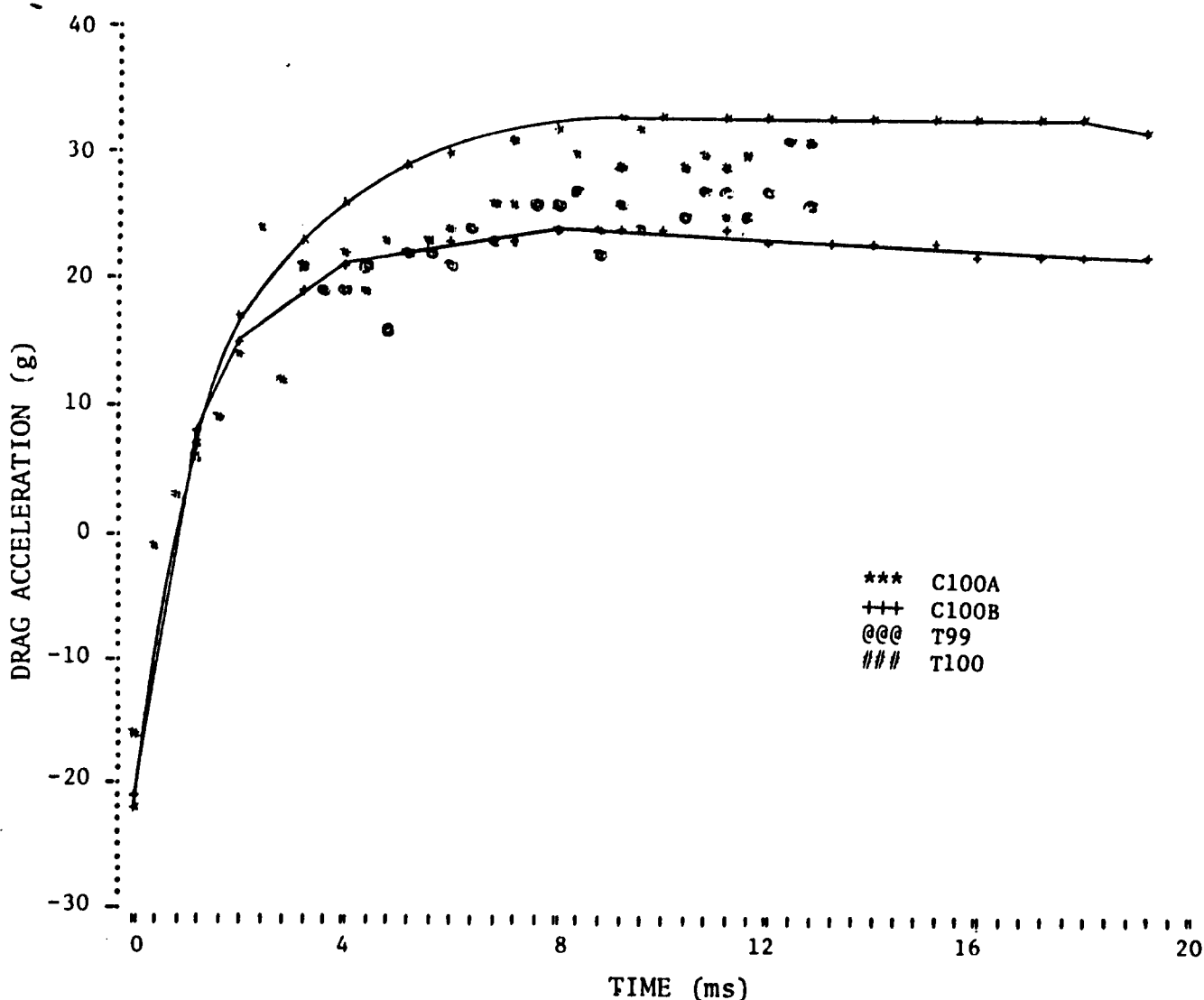


Figure 16. Calculated and experimental drag data for wood mitigator ($A_7 = 0.117 \text{ in.}^2$; shots 99 and 100).

4.3 Safety and Arming Device Tests

A current Army requirement is that a fuze shall not become functional (arm) until subjected to two distinct, unique environmental forces peculiar in the use of the fuze. One such double signature is provided by a safety and arming mechanism (S&A) that requires a successive setback and drag, in that order, during which time the S&A goes through three states: safe, to fail-safe, to fully armed. The setback S&A is required to be insensitive to a setback of 2500 g. An excessive setback of about 40,000 g can result in structural damage and malfunction. The fail-safe condition results when the S&A has experienced an adequate setback signature and the drag signature is inadequate or does not occur in the proper time sequence with respect to

the setback signature. For arming to occur, the simulation of aerodynamic drag (minimum amplitude of 3 g) must be initiated within about 5 ms following the termination of the setback, and the drag pulse must endure for a minimum time. The minimum pulse time decreases with increasing drag and amounts to 20 ms for a 3-g drag pulse. Moreover, the fuze must not arm at accelerations below 1 g regardless of pulse duration. Either an arm or a fail-safe condition results for drags between these limits.

As a demonstration of the feasibility of the simulator as a tester, a hollow bird was prepared to accommodate two S&A's (fig. 3). The total weight of the bird including two of the devices was brought up to the 0.53-kg weight of the bird in the tests previously described. The MEM's, washers, and mitigators were used so that the setbacks attained are assumed to be the same as those shown in figures 6 and 7.* However, the diameter of the new bird was slightly smaller, so that the A7 value associated with each washer was slightly larger. Drags up to 9 g were obtained. The shapes of the drag pulses are shown in figures 9 to 16. Streak photograph data were available for a total time of 20 ms for each test, including setback. The calculated drag pulse duration (corresponding to the MEM speed and the time required for the washer to exit from the catch tube) was 21 ms for the wood mitigator and 91 ms for the aluminum mitigator.

Table III summarizes the test results on the S&A. In all tests, the setbacks shown in figures 6 and 7 caused the device to proceed from a safe to a fail-safe position. Tests (not presented here) showed that the device would remain in the safe position when the bird impact speed was reduced to 95 ft/s (29 m/s) and the mitigator was aluminum. For this speed, the pulse duration or magnitude of the setback or both were insufficient to cause the S&A to proceed to the fail-safe position, which condition agrees with the above-noted design requirement for the S&A. Except in 1 out of 52 tests (wood mitigator with $A7 = 0.48 \text{ in.}^2 [3.1 \text{ cm}^2]$), the test data of table III indicate that the S&A performed as expected. Otherwise, with proper setback, the S&A armed as required when the drag was larger than 3 g and remained in the fail-safe position for a drag not exceeding 1 g.

**In the chronological order of this work, the simulator tests on the S&A were performed prior to the previously described measurements, and streak photograph data were not obtained. However, on the basis of the precision and repeatability of the data shown in figures 6 to 16, the setback data can be assumed to be the same as those shown in figures 6 and 7, and the predicted frictionless drag data ($C = 1$) should adequately represent test data.*

TABLE III. TEST RECORD OF PERFORMANCE OF FUZE SAFETY AND ARMING DEVICE

Mitigator	Tests (No.)	Cavity leakage area A7 (in. ²)	Fail-safe	Armed	Drag range (g)
Aluminum	16	0.15	0	16	9 to 3
	2	0.20	0	2	4 to 2
	6	0.30	5	1	2
	1	0.39	1	0	1
	2	0.48	2	0	0.9
	6	0.67	6	0	0.4
Wood	4	0.30	0	4	7 to 5
	8	0.48	1 ^a	7	4 to 3
	3	0.67	1	2	2
	4	1.49	4	0	0.3

^aIndicates malfunction of fuze device.

5. SUMMARY AND CONCLUSIONS

The setback and the drag were combined into a single laboratory tester to simulate, in the proper time frame, the sequential setback and the aerodynamic drag experienced by Army ordnance projectiles. In the present tests, the maximum setback was about 5000 g, and a steady-state drag commenced within 4 ms of the completion of the setback. An aerodynamic drag up to 30 g was simulated for 20 ms and up to 17 g for 90 ms.

Differences among test-to-test setback acceleration data for both wood and aluminum mitigators are generally within about 10 percent of the instantaneous average value.

Finally, tests were performed on several units of an S&A to demonstrate the feasibility of the simulator as a tester. The results of the simulator tests were found to be in good agreement with known design characteristics.

SYMBOLS

- A Instantaneous mitigator crush area (as measured at projectile ["bird"] interface) (in.²)
- An Acceleration (ft/s²)
- A7 Cavity leakage area, comprising sum of leakages between catch tube and momentum exchange mass (MEM) and between catch tube and bird (in.²)
- C Friction coefficient: = 0.5 (frictional), = 1.0 (frictionless)
- C1 Mitigator elongation at bird interface, arising from relaxing force thereon at T = TC (in.)
- C2 Mitigator elongation at MEM interface, arising from relaxing force thereon at T = TC (in.)
- D7 Air density (= 0.0749 lbm/ft³)
- F Mitigator dynamic crush force (lb)
- FO Mitigator static crush pressure (psi)
- LO Length of cavity at termination of setback (in.)
- Mn Mass (gram)
- M4 Crushed mitigator mass (lbm)
- M5 Uncrushed mitigator mass (lbm)
- M7 Mass of air passing into cavity (lbm)
- M4 Time rate of mitigator crush (lbm/s)
- n=1 Bird
- n=2 MEM
- n=3 Mitigator
- P Total air pressure in cavity (psi)
- PO Ambient atmospheric pressure (= 14.7 psi)

SYMBOLS (cont'd)

- P7 Partial pressure in cavity caused by air leakage into or out of cavity (psi)
- R Hydrodynamic crush force [= $M4(U1 - U2)$] (lb)
- R7 Time rate of mass flow into or out of cavity (lbm/s)
- S Ratio of crush front travel to depth of bird penetration
- T Time (s)
- TC Time duration of mitigator crush (s)
- Un Velocity (ft/s)
- U0 Initial bird velocity (ft/s)
- U7 Speed of air leakage passing into or out of cavity (referred to area A7) (ft/s)
- X1 Honeycomb elongation at bird interface (= $C1 - Y3 + Y1 \geq 0$) (in.)
- X2 Honeycomb elongation at MEM interface (= $C2 - Y2 + Y3 \geq 0$) (in.)
- Yn Displacement (in.)
- Z1 Honeycomb spring constant at bird interface, where A1 is acceleration at $T = TC$ (= $-A1M1/C1$) (lb/in.)
- Z2 Honeycomb spring constant at MEM interface, where A1 is acceleration at $T = TC$ (= $-A1M1/C2$) (lb/in.)
- ρ Density of uncrushed mitigator (lbm/ft³)
- \emptyset Washer diameter (in.)

APPENDIX A.--CODES

Computer codes SETBACK and DRAG were used to compute the sequential setback and the aerodynamic drag described in the main body of the report.

CODE 1. SETBACK

```

80 N=1 J=
85 PRINT "SHOT NUMBER IS":J
90 N=N+1 HIT AT MEM , J=0
95 N=N+1 HIT AT BIND. J<>0
100 G1=454*32.2
110 G=32000
120 K=1000
130 T1=5E-6
150 M1=1700/G1
160 M2=42000/G1
170 M3=.245*12.56*30/1728
190 A0=12.56
200 S=1.2
210 D=.245
240 PRINT "FO=: V1=: UO=: L=: J=":
250 INPUT FO,V1,UO,L,J
260 U1=UO
270 :00.00 0000.0 0000. 00.00 00.0 000.0 0.00 000.0 000.0 00.00
280 :00.00 00.0 000. 0.000 00.0 000. 0.000 000.0 0000.0
290 PRINT " TIME -A1 U1 Y1 A2 U2 Y2 F R A"
320 V=(U1-U2)/UO
330 M5=M3-M4
340 A=AO/L*(Y1-Y2)
350 IF A<AO GOTO 370
360 A=A0
370 F=1.05*FO*A/A0*(1+V1*V)
375 F=F*AO
380 H4=D*A*S*(U1-U2)/144
390 M4=M4+H4*T1
400 H4=H4*(U1-U2)
410 A1=(F+H)/(M1+M4)
415 IF J=0 GOTO 570
416 A1=(F)/(M1+M5)
570 A2=F/(M2+M5)
575 IF J=0 GOTO 630
576 A2=(F+H)/(M2+M4)
630 IF T<N*1E-4 GOTO 670
640 PRINT USING 270,T*1E+3,-A1/G,U1,Y1,A2/G,U2,Y2,F/K,H/K,A
650 IF U2>U1 GOTO 700
660 N=N+.5
670 T=T+T1
671 U1=U1+A1*T1
672 Y1=Y1+12*U1*T1
673 U2=U2+A2*T1
674 Y2=Y2+12*U2*T1
680 IF U2<U1 GOTO 320
690 GOTO 640
700 PRINT
705 N=T
710 PRINT "SPRING CONSTANTS C1,C2=":
720 INPUT C1,C2
740 U3=U1
750 Z1=-A1*M1/C1
760 Z2=-A1*C1/C2
770 PRINT " TIME -A1 U1 X1 A2 U2 X2 A3 U
780 Y1=Y2+Y3=0
790 X1=C1-Y3+Y1
800 IF X1>0 GOTO 820
810 X1=0
820 IF X1<C1 GOTO 850
830 U1=U1*(M1*(U1+M3*U1))/(M1+M3)
840 X1=C1
850 X2=C2-Y2+Y1
860 IF X2>0 GOTO 880
870 X2=0
880 IF X2<C2 GOTO 970
890 J1=U2*(M1*(U3+M2*U2))/(M1+M2)
900 X2=C2
970 A1=-Z1*X1/H1
980 A3=(Z1*X1-Z2*X2)/H3
1000 A2=Z2*X2/H2
1140 IF T<N GOTO 1220

```

APPENDIX A

CODE 1. SETBACK (Cont'd)

```

1150 PRINT USING 280, T*1E+3, -A1/G, U1, X1, A2/G, U2, X2, A3/G, U3
1200 IF #=1 GOTO 1260
1210 N=N+5E-5
1220 T=T+T1
1221 U1=U1+A1*T1
1222 U2=U2+A2*T1
1223 U3=U3+A3*T1
1224 Y1=Y1+12*U1*T1
1225 Y2=Y2+12*U2*T1
1226 Y3=Y3+12*U3*T1
1230 IF X1+X2>0 GOTO 790
1240 W=1
1250 GOTO 1150
1260 END

```

CODE 2. DRAG

```

100 G=32.2
105 G0=1/G
110 G1=454*G
120 m1=454/g1
130 m2=3800/g1
140 P1=PO-P2=14.7
150 TO=530
160 R=53.34
170 a6=3.14
190 T1=1E-4
190 PRINT "LO=: Pa; A7=: C=";
200 INPUT LO, P, A7, C
210 P6=P
220 U1=1
230 U2=15
240 V=A6*L0/1728
250 M6=P6*V/N*TO*144
270 D7=P0/N*TO*144
280 :###. ###.## ###.0 ##.## ##.## ##.0 ##.## ##.## ##.0 ##.0 ##.0
290 PRINT "TIME: A1 U1 Y1 A2 U2 Y2 M7 P7 U7 P"
291 PRINT USING 260, T*1E+3, A1*G0, U1, Y1, A2*G0, U2, Y2, M7*1000, P7, U7, P
292 T=T+T1
293 N=N+1
300 V1=A6*L1/1728
310 V=V+V1
320 P6=M6*N*TO/V/144
325 IF P0<P GOTO 335
330 U7=C*(2*(P0-P)*144*32.2/D7)`.5
331 GOTO 340
335 U7=-C*(2*(P-P0)*144*32.2/D7)`.5
340 M7=D7*U7*A7/144*T1
350 M7=M7+M7
360 P7=M7*N*TO/V/144
370 P=P6+P7
380 A1=(P0-P)*A6/M1
390 A2=(P-P2)*(A6-A7)/M2
400 U2=U2+A2*T1
410 Y2=Y2+12*U2*T1*12
420 U1=U1+A1*T1
430 Y1=Y1+12*U1*T1*12
440 L1=(U2-U1)*12*T1
450 IF T<N*1E-3 GOTO 490
460 PRINT USING 280, T*1E+3, A1*G0, U1, Y1, A2*G0, U2, Y2, M7*1000, P7, U7, P
470 IF #=1 GOTO 530
480 N=N+1
490 T=T+T1
500 IF T<10*1E-3 GOTO 300
510 W=1
520 GOTO 460
530 END

```

DISTRIBUTION

DEFENSE DOCUMENTATION CENTER
CAMERON STATION, BUILDING 5
ALEXANDRIA, VA 22314
ATTN DDC-TCA (12 COPIES)

COMMANDER
USA RSCH & STD GP (EUR)
BOX 65
FPO NEW YORK 09510
ATTN LTC JAMES M. KENNEDY, JR.
CHIEF, PHYSICS & MATH BRANCH

COMMANDER
US ARMY MATERIEL DEVELOPMENT
& READINESS COMMAND
5001 EISENHOWER AVENUE
ALEXANDRIA, VA 22333
ATTN DRXAM-TL, HQ TECH LIBRARY
ATTN DRCDE-A, PROGRAM SUPPORT OFFICE
ATTN DRCDE-R, SYS EVAL & TESTING
ATTN DRCDE-D, SYSTEMS DEV
ATTN DRCPA-E, ENVIRONMENTAL
CONTROL OFFICE
ATTN DRCQA, DIR FOR QUALITY ASSURANCE
ATTN DRCPM, PROJ OFF, ARMCOM
ATTN DRCSE-E, RESEARCH & ENGINEERING
ATTN DRCBSI-F, SYS DIR: ARTILLERY

COMMANDER
USA ARMAMENT COMMAND
ROCK ISLAND, IL 61201
ATTN DRSAR-ASF, FUZE DIV
ATTN DRSAR-PDF, SYS DEV DIV - FUZES

COMMANDER
USA MISSILE & MUNITIONS CENTER & SCHOOL
REDSTONE ARSENAL, AL 35809
ATTN ATSK-CTD-F

OFFICE OF THE DIRECTOR OF DEFENSE
RESEARCH & ENGINEERING
THE PENTAGON
WASHINGTON, DC 20301
ATTN TECHNICAL LIBRARY

OFFICE, CHIEF OF RESEARCH, DEVELOPMENT
& ACQUISITION
DEPARTMENT OF THE ARMY
WASHINGTON, DC 20310
ATTN DAMA-AR, DIRECTOR ARMY RESEARCH
ATTN DAMA-DD, DIRECTOR, DEVELOPMENTS

DEFENSE RESEARCH ESTABLISHMENT
VALCARTIER
DEFENSE RESEARCH BOARD
QUEBEC, CANADA
ATTN DIRECTOR OF R&D

DIRECTOR
DEFENSE RESEARCH AND ENGINEERING
THE PENTAGON
WASHINGTON, DC 20301
ATTN LIBRARY (TECHNICAL), 3C-128

ADVANCED RESEARCH PROJECTS AGENCY
1400 WILSON BLVD
ARLINGTON, VA 22209
ATTN MR. CLIFFORD F. MCLAIN,
MISSILE PHENOMENOLOGY BRANCH

ARMY ADVANCED BALLISTICS MISSILE
DEFENSE AGENCY
P.O. BOX 5474
RIVERSIDE, CA 92507
ATTN TECH DIRECTOR

COMMANDER
US ARMY BALLISTICS RESEARCH LABORATORIES
ABERDEEN PROVING GROUND, MD 21005
ATTN DEVELOPMENT & PROOF SERVICES,
SAUL TARAGIN
ATTN INTERIOR BALLISTICS LABORATORY
ATTN SIGNATURE & PROPAGATION LABORATORY
ATTN DRXBR-BB, V. RICHARD
ATTN DRXBR-BB, J. PILCHER
ATTN DRXBR-EB, W. MERMAGEN
ATTN DRXBR-EB, E. BOYER
ATTN STEAP-TL, TECHNICAL LIBRARY
DIVISION (2 COPIES)
ATTN TECHNICAL LIBRARY, BLDG 313
ATTN MR. E. BOYER, CHIEF,
TRANSONIC RANGE FACILITY

COMMANDER
US ARMY MOBILITY EQUIPMENT RESEARCH
& DEVELOPMENT CENTER
FORT BELVOIR, VA 22060
ATTN SMEFB-W, TECHNICAL LIBRARY

COMMANDER
US ARMY WEAPONS COMMAND
ROCK ISLAND, IL 61201
ATTN LIBRARY

COMMANDER
US ARMY MATERIALS & MECHANICS
RESEARCH CENTER
WATERTOWN, MA 02172
ATTN TECHNICAL INFORMATION CENTER

COMMANDER
YUMA PROVING GROUND
YUMA PROVING GROUND, AZ 85364
ATTN STEYP-TE, TEST &
EVALUATION DIRECTORATE

COMMANDER
US ARMY RESEARCH OFFICE (DURIAM)
P.O. BOX 1221
TRIANGLE RESEARCH PARK, NC 27709
ATTN CRD-AA-IP

COMMANDER
US ARMY TANK-AUTOMOTIVE CENTER
WARREN, MI 48090
ATTN SNOTA-RCI, INSTRUMENT-
ELECTRICAL LABORATORY

DISTRIBUTION (Cont'd)

US ARMY TANK-AUTOMOTIVE CENTER (Cont'd)
 ATTN SMOTA-RCH, MATERIALS LABORATORY
 ATTN SMOTA-RCS, PHYSICAL SCIENCES
 LABORATORY
 ATTN SMOTA-RCF, FIRE POWER LABORATORY

COMMANDER
 EUSTIS DIRECTORATE
 US ARMY AIR MOBILITY RESEARCH
 & DEVELOPMENT LABORATORY
 FORT EUSTIS, VA 23604
 ATTN DIRECTOR, R&D

COMMANDER
 US ARMY MOBILITY EQUIPMENT RESEARCH
 & DEVELOPMENT CENTER
 FORT BELVOIR, VA 22060
 ATTN TECHNICAL DOCUMENT CENTER

COMMANDER
 NAVAL SURFACE WEAPONS CENTER
 WHITE OAK, MD 20910
 ATTN A. SEIGAL
 ATTN V. F. DEVOST
 ATTN AIR GUN GROUP
 ATTN TECHNICAL LIBRARY

DEPARTMENT OF THE NAVY
 ORDNANCE SYSTEM COMMAND
 WASHINGTON, DC 20360
 ATTN DLI-3, TECHNICAL LIBRARY

DIRECTOR
 NAVAL RESEARCH LABORATORY
 WASHINGTON, DC 20390
 ATTN CODE 2620, TECH LIBRARY
 ATTN CODE 2027, LIBRARY
 ATTN CODE 2029, (ONRL)

COMMANDER
 NAVAL WEAPONS CENTER
 CHINA LAKE, CA 93557
 ATTN TECH LIBRARY
 ATTN CODE 406, TECH LIB

COMMANDER
 US NAVAL SURFACE WEAPONS CENTER
 DAHLGREN, VA 22448
 ATTN LEON ANDERSON
 ATTN LIBRARY
 ATTN CODE KE
 ATTN CODE TX

DIRECTOR
 US NAVAL ELECTRONICS LABORATORY
 CENTER
 SAN DIEGO, CA 92152

U. S. NAVAL ACADEMY
 ENGINEERING DEPT
 ANNAPOLIS, MD 21402
 ATTN LIBRARY

COMMANDER
 NAVAL UNDERSEA WARFARE CENTER
 SAN DIEGO DIVISION
 271 CATALINA BOULEVARD
 SAN DIEGO, CA 92152

COMMANDER
 US NAVAL AIR DEVELOPMENT CENTER
 WARMINSTER, PA 18974
 ATTN NADC LIBRARY

COMMANDER
 NAVAL UNDERSEA CENTER
 SAN DIEGO, CA 92132
 ATTN DIR A. G. FABULA, CODE 6005

OFFICER-IN-CHARGE
 NAVAL UNDERSEA CENTER
 3202 E. FOOTHILL BOULEVARD
 PASADENA, CA 91107
 ATTN DR. J. G. WAUGH, CODE 2542

CHIEF OF NAVAL RESEARCH
 DEPARTMENT OF THE NAVY
 ARLINGTON, VA 22217
 ATTN CODE 463
 ATTN CODE 438
 ATTN CODE 439

COMMANDER
 NAVAL AIR SYSTEMS COMMAND
 DEPARTMENT OF THE NAVY
 WASHINGTON, DC 20360
 ATTN AIR-03B
 ATTN AIR-5203
 ATTN AIR-5301
 ATTN AIR-5302

COMMANDER
 NAVAL SEA SYS COMMAND, HQ
 DEPARTMENT OF THE NAVY
 2521 JEFFERSON DAVIS HIGHWAY
 ARLINGTON, VA 20360
 ATTN NSEA-03A
 ATTN NSEA-035B
 ATTN NSEA-541
 ATTN NSEA-0521
 ATTN NSEA-0532

COMMANDING OFFICER
 NAVAL CIVIL ENGINEERING LABORATORY
 PORT HUENEME, CA 93041

COMMANDER
 NAVAL SHIP RESEARCH AND
 DEVELOPMENT CENTER
 CARDEROCK, MD 20034
 ATTN MISS ELIZABETH DEMPSEY, CODE 534
 ATTN MR. PAUL GRANVILLE, CODE 581
 ATTN MR. G. H. FRANZ
 ATTN MR. WILLIAM R. HOOVER
 ATTN MR. R. J. GRADY
 ATTN MR. D. CIESLOWSKI
 ATTN STRUCTURES

DISTRIBUTION (Cont'd)

COMMANDER
US NAVAL MISSILE CENTER
POINT MUGU, CA 93041
ATTN TECHNICAL LIBRARY, CODE NO322

AIR FORCE WEAPONS LABORATORY
WLRP
KIRTLAND AIR FORCE BASE, NM 87117
ATTN CAPT R. G. HENNING

COMMANDER
ARMAMENT DEVELOPMENT AND
TEST CENTER
EGLIN AFB, FL 32542

COMMANDER
ARNOLD ENGINEERING DEVELOPMENT CENTER
ARNOLD AIR FORCE STATION, TN 37389
ATTN LIBRARIAN

COMMANDER
AF FLIGHT DYNAMICS LAB
WRIGHT-PATTERSON AFB, OH 45433
ATTN PTS SURVIVABILITY/VULNERABILITY
BRANCH

COMMANDER
ARNOLD ENGINEERING DEVELOPMENT CENTER
ARNOLD AIR FORCE STATION
TULLAHOMA, TN 37389
ATTN CAPT CARLOS TIRRES, DYR

AF OFFICE OF SCIENTIFIC RESEARCH
1400 WILSON BLVD
ARLINGTON, VA 22209
ATTN LIBRARIAN

COMMANDER
US ARMY MISSILE COMMAND
FRANKFORD ARSENAL
PHILADELPHIA, PA 19137
ATTN J4000, ARTILLERY AMMUNITION LAB
ATTN K1000, TECHNICAL LIBRARY, 0270
ATTN A6100, J. T. HUNT

COMMANDER
PICATINNY ARSENAL
DOVER, NJ 07801
ATTN SARPA-SCIENTIFIC & TECHNICAL
INFORMATION BRANCH
ATTN SARPA-TW3, W. HADOWANETZ
ATTN R. BUXTON
ATTN S. KOCH
ATTN F. SAXE

COMMANDER
EDGEWOOD ARSENAL
EDGEWOOD ARSENAL, MD 21010
ATTN TECHNICAL LIBRARY

US LIBRARY OF CONGRESS
SCIENCE & TECHNOLOGY DIVISION
WASHINGTON, DC 20540

NATIONAL BUREAU OF STANDARDS
WASHINGTON, DC 20234
ATTN LIBRARY
ATTN DR. GALEN B. SCHUBAUER

BOULDER LABORATORIES
NATIONAL BUREAU OF STANDARDS
BOULDER, CO 90302
ATTN LIBRARY

SANDIA LABORATOIRES
P.O. BOX 5800
ALBUQUERQUE, NM 87115
ATTN S. FLUENT
ATTN TECHNICAL LIBRARY
ATTN W. V. HEREFORD, DIV 7215
ATTN R. C. MAYDEW, AERO-THERMODYNAMICS
DEPT

SANDIA LABORATORIES
LIVERMORE LABORATORY
P.O. BOX 969
LIVERMORE, CA 04550
ATTN TECHNICAL REFERENCE LIBRARY

DIRECTOR
LAWRENCE RADIATION LABORATORY
P.O. BOX 1663
LOS ALAMOS, NM 87544
ATTN LIBRARIAN

JET PROPULSION LABORATORY
4800 OAK GROVE DRIVE
PASADENA, CA 91103
ATTN LIBRARY, TDS- N. E. DEVERAUX

NATIONAL ACADEMY OF SCIENCES
NATIONAL RESEARCH COUNCIL
COMMITTEE ON UNDERSEA WARFARE
2101 CONSTITUTION AVENUE, NW
WASHINGTON, DC 20418

NATIONAL AERONAUTIC AND SPACE ADMINISTRATION
LEWIS RESEARCH CENTER
21000 BROOKPARK ROAD
CLEVELAND, OH 44135
ATTN MR. GEORGE MANDEL, CHIEF, LIBRARY

NATIONAL AERONAUTICS AND SPACE
ADMINISTRATION
GODDARD SPACE FLIGHT CENTER
GREENBELT, MD 20771
ATTN LIBRARY
ATTN MR. E. F. SARGENT, CODE 67.2
ATTN DR. R. LEHNERT, CODE 530

NATIONAL AERONAUTICS AND SPACE
ADMINISTRATION
GEORGE C. MARSHALL SPACE FLIGHT CENTER
HUNTSVILLE, AL 35812
ATTN MR. H. A. CONNELL, R-P & VE-PT
ATTN DR. ERNST GEISSLER,
AERO-ASTRODYNAMICS LAB

DISTRIBUTION (Cont'd)

NATIONAL AERONAUTICS AND SPACE
ADMINISTRATION
LANGLEY RESEARCH CENTER
LANGLEY STATION
HAMPTON, VA 23365
ATTN LIBRARY, MS 185
ATTN MR. MITCHEL H. BERTRAM, MS 243
ATTN MR. RUSSELL HOPKO, FARD, MS 213

NATIONAL AERONAUTICS AND SPACE
ADMINISTRATION
600 INDEPENDENCE AVENUE, SW
WASHINGTON, DC 20546
ATTN DR. H. H. KURWEG, DIRECTOR
OF RESEARCH

NASA SCIENTIFIC AND TECHNICAL
INFORMATION FACILITY
P.O. BOX 33
COLLEGE PARK, MD 20740
ATTN NASA REPRESENTATIVE (SAK/DL)

COMMANDER
NATICK LABORATORIES
NATICK, MA 01762
ATTN DIRECTOR, R&D

FRANKLIN INST RESEARCH LABS
20TH & BENJAMIN FRANKLIN PARKWAY
PHILADELPHIA, PA 19103
ATTN TECHNICAL DIRECTOR

CORNELL UNIVERSITY
SCHOOL OF CHEMICAL ENGINEERING
GRUMAN HALL
ITHACA, NY 14850
ATTN E. L. RESLER, JR.

UNIVERSITY OF PITTSBURGH
ORDNANCE RESEARCH STAFF
520 DUPONT CIRCLE BLDG
1345 CONNECTICUT AVENUE, NW
WASHINGTON, DC 20036
ATTN F. GORDON BARBER

STANFORD RESEARCH INSTITUTE
ATTN SECURITY OFFICER
333 RAVENWOOD AVENUE
MENLO PARK, CA 94025

WASHINGTON STATE UNIVERSITY
R. L. ALBROOK HYDRAULIC LABORATORY
DIVISION OF INDUSTRIAL RESEARCH
PULLMAN, WA 91634
ATTN CHAIRMAN, MECHANICAL
ENGINEERING DEPT

MASSACHUSETTS INSTITUTE OF TECHNOLOGY
HYDRODYNAMICS LABORATORY
CAMBRIDGE, MA 02139
ATTN PROFESSOR A. T. IPPEN

UNIVERSITY OF ILLINOIS
COLLEGE OF ENGINEERING
DEPARTMENT OF THEORETICAL AND
APPLIED MECHANICS
212 TALBOT LABORATORY
URBANA, IL 61801
ATTN DR. J. M. ROBERTSON

CALIFORNIA INSTITUTE OF TECHNOLOGY
JET PROPULSION LABORATORY
PASADENA, CA 91103
ATTN MR. T. KICENIUK,
HYDRODYNAMICS LABORATORY
ATTN PROFESSOR M. S. PLESSET, DIV
OF ENGINEERING
ATTN PROFESSOR T. Y. WU

THE CATHOLIC UNIVERSITY OF AMERICA
DEPARTMENT OF SPACE SCIENCE
AND APPLIED PHYSICS
WASHINGTON, DC 20017
ATTN DR. C. C. CHANG

OHIO STATE UNIVERSITY
DEPARTMENT OF AERO-ASTRONAUTICAL
ENGINEERING
2036 NEIL AVENUE
COLUMBUS, OH 43210
ATTN PROFESSOR TING YI LI

UNIVERSITY OF MARYLAND
DEPARTMENT OF AEROSPACE ENGINEERING
GLEN L. MARTIN INSTITUTE OF TECHNOLOGY
COLLEGE PARK, MD 20742
ATTN PROFESSOR JOHN D. ANDERSON, JR.

COLORADO STATE UNIVERSITY
FORT COLLINS, CO 80521
ATTN CIVIL ENGINEERING HYDRAULICS
LABORATORY

UNIVERSITY OF UTAH
COLLEGE OF ENGINEERING
SALT LAKE CITY, UT 84112
ATTN PROFESSOR MAX L. WILLIAMS, DEAN

STATE UNIVERSITY OF NEW YORK AT BUFFALO
DEPARTMENT OF MECHANICAL ENGINEERING
FACULTY OF ENGINEERING AND APPLIED SCIENCES
PARK ENGINEERING BUILDING
BUFFALO, NY 14212
ATTN J. GORDON HALL

DIRECTOR ORDNANCE RESEARCH LABORATORY
PENNSYLVANIA STATE UNIVERSITY
P.O. BOX 30
STATE COLLEGE, PA 16801

UNIVERSITY OF MARYLAND
MECHANICAL ENGINEERING DEPARTMENT
COLLEGE PARK, MD 20742
ATTN DR. C. L. SAYRE
ATTN PROFESSOR A. WILEY CHERWOOD
ATTN DR. JAMES DALLY

DISTRIBUTION (Cont'd)

UNIVERSITY OF CALIFORNIA
DEPARTMENT OF NAVAL ARCHITECTURE
BERKELEY, CA 94720
ATTN PROFESSOR J. V. WEHAUSEN

THE UNIVERSITY OF IOWA
THE INSTITUTE OF HYDRAULIC RESEARCH
IOWA CITY, IA 52240
ATTN HUNTER ROUSE
ATTN LOUIS LANDWEBER

GEORGIA INSTITUTE OF TECHNOLOGY
ENGINEERING EXPERIMENT STATION
225 NORTH AVENUE, NW
ATLANTA, GA 30332
ATTN HYDRAULICS LABORATORY

WORCESTER POLYTECHNIC INSTITUTE
ALDEN RESEARCH LABORATORY
WORCESTER, MA 01609
ATTN PROFESSOR L. J. HOOPER
ATTN L. C. NEALE

SUPERINTENDENT
NAVAL POSTGRADUATE SCHOOL
MONTEREY, CA 93940
ATTN LIBRARY, CODE 2124

JOHNS HOPKINS UNIVERSITY
APPLIED PHYSICS LABORATORY
8621 GEORGIA AVENUE
SILVER SPRING, MD 20910
ATTN DR. L. L. CRONVICH
ATTN DOCUMENT LIBRARIAN
ATTN MR. L. B. WECKESSER

UNIVERSITY OF CALIFORNIA
LOS ALAMOS SCIENTIFIC LABORATORY
P.O. BOX 1663
LOS ALAMOS, NM 97544
ATTN REPORT LIBRARY

UNIVERSITY OF WYOMING
COLLEGE OF ENGINEERING
UNIVERSITY STATION, BOX 3295
LARAMIE, WY 82070
ATTN ENGINEERING LIBRARY
ATTN PROFESSOR JAMES D. MATHENY
HEAD DEPT OF MECHANICAL
ENGINEERING

UNIVERSITY OF DELAWARE
MECHANICAL AND AERONAUTICAL
ENGINEERING DEPARTMENT
NEWARK, NJ 19711
ATTN DR. JAMES DANBERG

DIRECTOR
SOUTHWEST RESEARCH INSTITUTE
DEPARTMENT OF MECHANICAL SCIENCES
SAN ANTONIO, TX 78206
ATTN LIBRARY

STANFORD, UNIVERSITY
STANFORD, CA 94305
ATTN PROFESSOR E. Y. HSU
ATTN DR. DANIEL BERSHADER
DEPT OF AERONAUTICAL AND
ASTRONAUTICAL

UNIVERSITY OF MINNESOTA
ST. ANTHONY FALLS HYDRAULIC
MISSISSIPPI RIVER AT 3RD AVE WE
MINNEAPOLIS, MN 55141
ATTN PROFESSOR E. SILBERMAN

STEVENS INSTITUTE OF TECHNOLOGY
DAVIDSON LABORATORY
HOBOKEN, NJ 07030
ATTN DR. ALBERT STRUMPF
ATTN MR. ANTHONY SUAREZ

UNIVERSITY OF WEST FLORIDA
FACULTY OF AERONAUTICAL SYSTEMS
PENSACOLA, FL 32504
ATTN DR. RICHARD FLEDDERMAN

HONEYWELL ORDNANCE DIVISION
600 2ND STREET, N.
HOPKINS, MN 53343
ATTN E. M. JOHNSON
ATTN P. T. KERSH
ATTN MR. S. SOPSZAK

MELPAR, INC.
888 17TH STREET, NW
WASHINGTON, DC 20006

HEXCEL CORPORATION
LOYOLA FEDERAL BLDG
BEL AIR, MD 21014
ATTN MR. T. EMERSON

PHYSICS INTERNATIONAL COMPANY
2700 MERCED STREET
SAN LEANDRO, CA 94577

SYSTEMS, SCIENCE AND SOFTWARE
P.O. BOX 1620
LA JOLLA, CA 92037
ATTN LIBRARIAN

GENERAL MOTORS
TECHNICAL CENTER
WARREN, MI 48090
ATTN LIBRARIAN

BOEING COMPANY, THE
RESEARCH AND ENGINEERING DIV
SEATTLE, WA 98100
ATTN LIBRARIAN

GOODYEAR AEROSPACE CORP
AKRON, OH
ATTN LIBRARIAN

DISTRIBUTION (Cont'd)

MARTIN MARIETTA CORP
AEROSPACE DIV
P.O. BOX 5837
M.D. 109
ORLANDO, FL 32805
ATTN LIBRARIAN

AEROPHYSICS COMPANY
3500 CONNECTICUT AVENUE NW
WASHINGTON, DC 20003
ATTN MR. GABRIEL D. BOEHLER

OCEANICS, INC.
PLAINVIEW, LONG ISLAND, NY 11803
ATTN DR. PAUL KAPLAN

THERM ADVANCED RESEARCH, INC.
100 HUDSON CIRCLE
ITHACA, NY 14851

KAMAN SCIENCES CORP
KAMAN NUCLEAR DIVISION
P.O. BOX 7463
COLORADO SPRINGS, CO 80901
ATTN DR. A. P. BRIDGES

LOCKHEED MISSILES AND SPACE COMPANY
MISSILE SYSTEMS DIVISION
P.O. 504
SUNNYVALE, CA 94088
ATTN R. W. KERMEN, DEPT 50-35,
BLDG 153 F/1
ATTN FRANK CHAPMAN, DEPT 81-90

NORTH AMERICAN AVIATION INC
SPACE AND INFORMATION SYSTEMS DIVISION
DOWNEY, CA 90241
ATTN TECHNICAL INFORMATION CENTER,
D/096-722 (AJ01)

GENERAL DYNAMICS
ELECTRIC BOAT DIVISION
MARINE TECHNOLOGY CENTER
P.O. BOX 911
SAN DIEGO, CA 92112
ATTN MR. W. B. BARKLEY
ATTN DR. BLANE R. PARKIN,
MAIL ZONE 6-114

AVCO-EVERETT RESEARCH LABORATORY
885 REVERE BEACH PARKWAY
EVERETT, MA 02149
ATTN DR. ARTHUR KANTROWITZ

BATTELLE MEMORIAL INSTITUTE
505 KING AVENUE
COLUMBUS, OH 43201
ATTN REMOTE AREA CONFLICT
INFORMATION CENTER

BOEING COMPANY
AEROSPACE COMPANY
P.O. BOX 3707
SEATTLE, WA 98124
ATTN 8K-38, RUTH E. PERRENBOOM

ALLEGHANY BALLISTICS LABORATORY
HERCULES POWDER COMPANY
CUMBERLAND, MD 12502
ATTN CAPTAIN N. J. KLEISS

AEROSPACE CORPORATION
P.O. BOX 95085
LOS ANGELES, CA 90045
ATTN DR. J. S. WHITTIER
ATTN MR. M. J. ADAMS

GENERAL ELECTRIC COMPANY
SPACE DIVISION
P.O. BOX 8555
PHILADELPHIA, PA 19101
ATTN MR. LAWRENCE I. CHANSEN,
MANAGER/MSC LIBRARIES
ATTN MR. ANTHONY P. COPPA
ATTN MR. R. F. PAPA

GENERAL ELECTRIC COMPANY
RE-ENTRY AND ENVIRONMENTAL SYSTEMS
DIVISION
P.O. BOX 722
PHILADELPHIA, PA 19101
ATTN MR. W. DASKIN, MANAGER, TECHNOLOGY
ENGINEERING SECTION
ATTN MR. W. W. WILSON, MANAGER MILITARY
OCEAN PROGRAMS

GENERAL ELECTRIC COMPANY
VALLEY FORGE SPACE TECHNOLOGY CENTER
KING OF PRUSSIA, PA 19406
ATTN MR. L. MARSHALL
ATTN DR. S. WOODALL
ATTN DR. R. F. HOPPMANN

GRUMMAN AEROSPACE CORPORATION
SOUTH OYSTER BAY ROAD
BETHPAGE, LONG ISLAND, NY 11714
ATTN MR. GEUSEPPE AVALLONE

UNITED AIRCRAFT CORPORATION
RESEARCH LABORATORY
EAST HARTFORD, CT 06108
ATTN MR. J. J. CHARETTE
ATTN MR. F. S OWEN

IIT RESEARCH INSTITUTE
10 W. 35TH STREET
CHICAGO, IL 60616
ATTN LIBRARIAN

DISTRIBUTION (Cont'd)

TERA TEK, INC
420 WAKARA WAY
UNIVERSITY OF UTAH RESEARCH PARK
SALT LAKE CITY, UT 84109
ATTN SIDNEY GREEN

HYDRONAUTICS, INC.
PINDELL SCHOOL ROAD
HOWARD COUNTY
LAUREL, MD 20810
ATTN MR. P. EISENBERG
ATTN MR. M. P. TULIN

HARRY DIAMOND LABORATORIES
ATTN LOWREY, AUSTIN, III, COL, COMMANDER/
FLYER, I.N./LANDIS, P.E./
SOMMER, H./OSWALD, R. B.
ATTN CARTER, W.W., DR., TECHNICAL
DIRECTOR/MARCUS, S.M.
ATTN KIMMEL, S., PAO
ATTN CHIEF, 0021
ATTN CHIEF, 0022
ATTN CHIEF, LAB 100
ATTN CHIEF, LAB 200
ATTN CHIEF, LAB 300
ATTN CHIEF, LAB 400
ATTN CHIEF, LAB 500
ATTN CHIEF, LAB 600
ATTN CHIEF, DIV 700
ATTN CHIEF, DIV 800
ATTN CHIEF, LAB 900
ATTN CHIEF, LAB 1000
ATTN RECORD COPY, BR 041
ATTN HDL LIBRARY (5 COPIES)
ATTN CHAIRMAN, EDITORIAL COMMITTEE
ATTN CHIEF, 047
ATTN TECH REPORTS, 013
ATTN PATENT LAW BRANCH, 071
ATTN GIDEP OFFICE, 741

HARRY DIAMOND LABORATORIES (Cont'd)
ATTN LANHAM, C., 0021
ATTN RICHMOND, L. 420
ATTN BETTWEY, D., 710
ATTN BOCCIA, M., 420
ATTN DAVIS, H., 850
ATTN JOHNSON, R., 650
ATTN OVERMAN, D., 420
ATTN ZASTROW, K., 741
ATTN CULLINANE, J., 620
ATTN SPELLMAN, J., 0021
ATTN MILLER, J., 620
ATTN HUM, S., 0023
ATTN SNYDER, G., 940
ATTN MORROW, D., 410
ATTN MOY, C., 0611
ATTN COOKE, E., 430
ATTN COSMAN, M., 420
ATTN BEARD, J., 420
ATTN SMITS, W., 650
ATTN SIMMONS, E., 940
ATTN BLODGETT, F., 940
ATTN KUPER, W., 940
ATTN BALL, A., 850
ATTN CURCHACK, H., 850
ATTN KAYSER, R., 850
ATTN MARY, D., 850
ATTN NELSON, F., 850
ATTN TEVELOW, F., 850
ATTN BIGGAR, A., 940
ATTN LUCEY, G., 750
ATTN TURRILL, F., 940
ATTN LEASURE, W., 430
ATTN BILBROUGH, H., 420
ATTN ANSTINE, C., 620
ATTN BORING, S., 620
ATTN OTTEN, M., 0022
ATTN SABONIS, A., 940
ATTN WESTLUND, R., 640
ATTN POLLIS, I. (20 COPIES)